JOURNAL OF GEOPHYSICAL RESEARCH, VOL. 97, NO. A4, PAGES 4143–4161, APRIL 1, 1992

The Distribution of Atomic Hydrogen in the Magnetosphere of Saturn

D. E. SHEMANSKY[1] AND D. T. HALL

Lunar and Planetary Laboratory, University of Arizona, Tucson

Three sets of previously unpublished Voyager ultraviolet spectrometer (UVS) observations in H Ly α emission reveal a complex three-dimensional distribution of atomic hydrogen in the Saturn system. Voyager 1 observations during the postencounter period have provided a map of the distribution looking down on the equatorial plane. The reduced data show a nonuniform distribution in local time with a preponderance of emission on the duskside. The emission extends radially inward to the top of the Saturn atmosphere with stronger signals appearing close to the planet strongly suggesting that the principal source is the sunlit Saturn atmosphere. In the subsolar sector of the magnetosphere no excess emission in the vicinity of Titan's orbit is detectable. But a peak in the emissions near 20 Saturn radii (R_S) appears in the antisolar sector suggesting a significant contribution from Titan. Voyager 1 and 2 preencounter observations also show H Ly α emissions increasing monotonically toward the planet but with a distinctive dawnside excess. The preencounter and postencounter results may be reconciled if there exists a complex H gas distribution with significant radial and azimuthal variations. We conclude that the preliminary results reporting a toroidal hydrogen distribution with a cavity inside 8 R_S (Broadfoot et al., 1981) are invalid because of limited spatial resolution and poor statistics. The fact that the hydrogen distribution joins continuously into the atmosphere of Saturn and shows significant azimuthal variations indicates that the dominant source inside 8 R_S is in the Saturn exosphere. The local time character and magnitude of the distribution could be produced by ballistic and escaping atoms originating in the sunlit exosphere. The energies required for the source atoms can be obtained by electron excitation of H_2 within a scale height of and above the exobase. The total rate of production of atomic hydrogen may be as much as 3 times larger than that inferred earlier from the observed brightness of H_2 EUV radiation from the equatorial atmosphere. The deposition of heat at the top of the thermosphere by the atomic hydrogen source can account for the measured temperature. We have examined the impact of the conditions imposed by the measured content of neutrals and ions in the inner magnetosphere through model calculations. We predict in a preliminary analysis that the neutral gas in the low latitude region of the inner magnetosphere is dominated by water products. A typical calculation shows [O] $\sim$ 400 cm^{-3}, [OH] $\sim$ 40 cm^{-3}, [H] $\sim$ 130 cm^{-3}, [O^+] $\sim$ 30 cm^{-3}, [H^+] $\sim$ 3 cm^{-3}, in the plasma sheet near 4.5 R_S; a mix of neutrals and ions of this order is required to balance the energy budget.

INTRODUCTION

Atomic hydrogen in the magnetosphere of Saturn has a major effect as both a source of ions loading the system with mass and as a limiting factor to the development of the plasmasphere. The presence of significant amounts of hydrogen was predicted by *McDonough and Brice* [1973], who argued that a substantial atmosphere on Titan should generate a measurable neutral torus at 20 Saturn radii (R_S). At that time Titan's upper atmosphere was considered to be mostly hydrogen and the escape rate would therefore be very large. The considerations requiring a heavy atmosphere were established later [*Hunten*, 1977]. It was generally assumed that the neutral hydrogen subsequently detected in the magnetosphere in 1975 by *Weiser et al.* [1977] originated in the Titan atmosphere. Several years later *Shemansky and Smith* [1982] argued on the basis of Voyager spacecraft data that Saturn is a major contributor [see *Hilton and Hunten*, 1988]. Other neutrals such as water group species from the inner satellites and nitrogen from Titan (probably mostly in atomic form) are also very likely present but have never been detected.

Other evidence has been obtained with the Copernicus satellite [*Barker et al.*, 1980] and the Pioneer 11 spacecraft [*Judge et al.*, 1979] indicating the presence of H near the rings and in the vicinity of Titan's orbit. However, *Clarke et al.* [1981] failed to detect an extended distribution at the rings or near Titan's orbit in IUE observations in May 5-9, 1980, to within $\pm$200 Rayleigh (R). Definitive results were finally obtained in Voyager spacecraft observations in November 1980 and August 1981, which provided one-dimensional radial distributions integrated parallel to the orbital plane. The description of the distribution in a preliminary analysis by *Broadfoot et al.* [1981] was one of a uniform torus extending to $\approx$25 R_S with a cavity inside 8 R_S. The presence of a cavity was predicted theoretically if one assumed that Titan was the source of the atomic hydrogen with most of the population in satellite orbits. Also the region inside 8 R_S was known to be elevated in plasma density suggesting relatively short H atomic lifetimes. Titan was a natural choice as a source [*McDonough and Brice*, 1973] because it had a known substantial atmosphere with a small escape velocity. The inner satellites and the rings have also been considered as both plasma and neutral sources through particle and photon sputtering of icy surfaces [*Carlson*, 1980; *Ip*, 1984; *Eviatar*, 1984; *Richardson et al.*, 1986; *Richardson and Eviatar*, 1987], but rates for these processes are limited. *Johnson* [1989] has predicted much larger sputtering rates.

Shemansky and Smith [1982] argued that an electron-excited atmosphere near the exobase at Saturn would produce energetic atomic hydrogen through various dissociation reactions. Subsequent analysis of Voyager 2 data indicated that the atomic hydrogen in fact extended into the plane-

[1]Now at Department of Aerospace Engineering, USC, Los Angeles.

Paper number 91JA02805.
0148-0227/92/91JA-02805$05.00

tary atmosphere [*Shemansky et al.*, 1985] and suggested that Uranus may show a similar effect [see *Shemansky and Smith*, 1986; *Shemansky and Hall*, 1987]. *Hilton and Hunten* [1988], on the basis of Voyager measurements of the extent of the gas above the satellite orbital plane, also concluded that Saturn must be the dominant source of hydrogen inside ≈10 R_S. The dissociation processes at the top of the thermosphere are a source of heat, and we briefly discuss the implied rate below.

The data presented in this article consist of three sets of previously unpublished Voyager ultraviolet spectrometer (UVS) observations of the Saturn system conducted by both spacecraft. First, extensive postencounter mosaic scans performed by Voyager 1 are presented in the form of an image of the partially open system looking down toward the north pole of the planet. Second, a set of preencounter scans conducted by each spacecraft is presented. These do not support the interpretation by *Broadfoot et al.* [1981] of a cavity in the hydrogen distribution inside 8 R_S. We review the Voyager 1 preencounter scans used by *Broadfoot et al.* [1981] and conclude that the complicated scan geometry and limited spatial resolution does not justify such a conclusion. All of the data presented here show significant H Ly α intensities within a few R_S of the planet.

We have examined the impact of the measured amounts of atomic hydrogen on the plasma sheet in the inner magnetosphere. The plasma content in this region has been constrained by an analysis of the Voyager Plasma Science experiment [*Richardson and Sittler*, 1990] . We discuss the reactions controlling the plasma assuming a source derived from the icy satellites. The dominance by heavy ions of mass-per-charge ratio near that of O^+, along with energy budget considerations, requires significant populations of the heavy water product neutrals at low latitudes, according to the analysis discussed below.

Voyager UVS Observations of the Saturn System

Voyager 1 Postencounter

Extensive Voyager 1 H Ly α emission measurements were performed during the Saturn 6 to 25-day postencounter period, 1980 day of year (DOY) 324–343 in the form of mosaic scans across the system. We have compiled these data and constructed an image of the system in 1216 Å radiation. The planet-spacecraft range extended from 140 to 55 R_S over the observational period, with the line of sight intersecting the satellite orbital plane at an angle of about 26°, looking down on the north pole of the planet. Figure 1*a* is a half tone plot of the accumulated reduced data. Both Saturn and Titan's orbital ellipse are illustrated in the figure for reference. The direction of the incident solar flux is shown by an arrow, and the terminator of Saturn is indicated by a line drawn where the terminator plane and the equatorial plane intersect. In the upper right-hand corner the Voyager UVS field of view is illustrated with the approximate orientation maintained during the mosaic scans. The intensity scale ranges in brightness from 250 R downward as indicated in Figure 1*a*. A background Ly α signal of ≈1300 R from the local interstellar medium (LISM) calculated using the *Ajello et al.* [1987] model has been subtracted from the data. In addition, an estimated contribution from stellar sources is removed from affected areas. (The data reduction process, background subtraction and noise levels are discussed in Appendix A.) A depression in the signal centered on the Saturn dark side atmosphere, defined approximately by the mean size of the instrument field of view, is caused by the occultation of the LISM flux by the planet. The dark side atmospheric emission rate is $I \approx 500$ R (*D. E. Shemansky*, unpublished manuscript, 1989), compared to the LISM background of ≈1300 R. Only a small contribution from the sunlit planetary atmosphere is detectable because the viewing direction is dominated by the dark hemisphere (see Figure 2). The most striking aspect of the image is the distinct asymmetry in the distribution with a maximum aligned approximately with the dusk terminator and a minimum in the predawn region. Most of the emission is confined inside Titan's orbit. The data were accumulated over a time interval corresponding to ≈1¼ Titan orbital periods. There appears to be a measurable indication of excess emission near Titan's orbit on the antisolar side of Saturn. The bright spot near the right ansa of Titan's orbit shown in Figure 1*a* may be caused by an imperfect correction for a stellar source in the background (see Appendix A). Bright patches toward the periphery of Figure 1*a* lose statistical significance because of lower integration times and poor signal-to- noise ratios. Figure 1*b* shows a half tone plot of the 1σ statistical noise level in one-to-one correspondence with the pixels in Figure 1*a*. Because these scans focused on the interior portion of the system, the error levels are reduced in the vicinity of Saturn relative to the peripheral regions. The bright region in Figure 1*a* within 2 R_S of the sunlit side of the planet can be entirely accounted for by emission from the sunlit crescent (average crescent surface brightness ≈4 kR). The observational geometry with respect to the terminator and the location of the rings is shown in Figure 2.

Regions showing brightness greater than 200 R are extensive on the duskside of the system within 10 R_S of the planet in Figure 1*a*. The UVS intensities obtained in the Voyager 1 preencounter period, giving line of sight integrations essentially in the orbital plane, are ≈150 R at the same (≈10 R_S) radial location [*Broadfoot et al.*, 1981]. An upward correction of 8% to this value due to differences in mean solar flux between observations implies that the abundance of atomic hydrogen on the duskside of the system is comparable in the Voyager 1 preencounter and postencounter perspectives. The H Ly α postencounter differential solar flux at line center is estimated to be $F_\lambda = 3.5 \times 10^{11}$ Ph cm^{-2} s^{-1} Å^{-1} (total flux $F = 3.6 \times 10^{11}$ Ph cm^{-2} s^{-1}) giving a value for the scattering probability of 1.8×10^{-3} s^{-1} at 1 AU. The H density inward of the 10 R_S radial position on the sunlit side of the planet is then [H] ≈ 100 cm^{-3}, assuming a pathlength of 16 R_S. This abundance corresponds to an optical depth of $\tau \approx 2$ if we assume an effective temperature of $T = 1000$ K for the gas. However, the velocity distribution of the gas will probably not be defined by Boltzmann statistics, as discussed below.

The distribution of the emission shown in Figure 1*a* is distinctly different from expectation for a torus centered on Titan's orbit. Figure 3 shows a simulation of the expected image if Titan were the sole source producing a torus of the dimensions described by *Broadfoot et al.* [1981].

Figure 4 shows a plot of the mean H Ly α intensities from Figure 1*a* summed in local time into 30° sectors inside 18 R_S. The intensity modulation is almost a factor of 2 with the peak occurring in the dusk sector. (The distribution outside 22 R_S suffers more from a low signal-to-noise ratio but shows no statistically significant modulation in local time.)

Fig. 1*a*. Half tone plot of the Saturn system in H Ly α emission obtained from Voyager 1 UVS mosaic scans of the system conducted during the period 1980 DOY 324–343 (6–25 days postencounter). The brightness scale in Rayleighs is given in the figure. The total integration time for the observations was 126 hours. The pixel size is 1 R_S x 1 R_S perpendicular to the spacecraft-planet line, 1 R_S x 2.4 R_S projected onto the satellite orbital plane. The angle between the spacecraft-planet line and the orbital plane is 26°. The data are shown after subtraction of the LISM background and stellar sources. The bright spot at the right ansa of Titan's orbit may be due to imperfect correction for one of the stellar sources. The location of the Sun-planet line is indicated in the upper right sector. The planet is drawn to size on the figure. The mean size and orientation of the Voyager UVS field of view is shown in the upper right corner. A small sunlit crescent affects the signal on the right side of the planet (see text, Figure 2). The data have been smoothed in a 3 × 3 pixel area, weighted by integration time. The depression in signal in a rectangular area oriented parallel to the length of the slit at the position of the planet is caused by occultation of the brighter background LISM by the planet. Bright and patchy areas toward the periphery and in some locations in the vicinity of Titan's orbit on the left side lose their significance because of low signal-to- noise ratios.

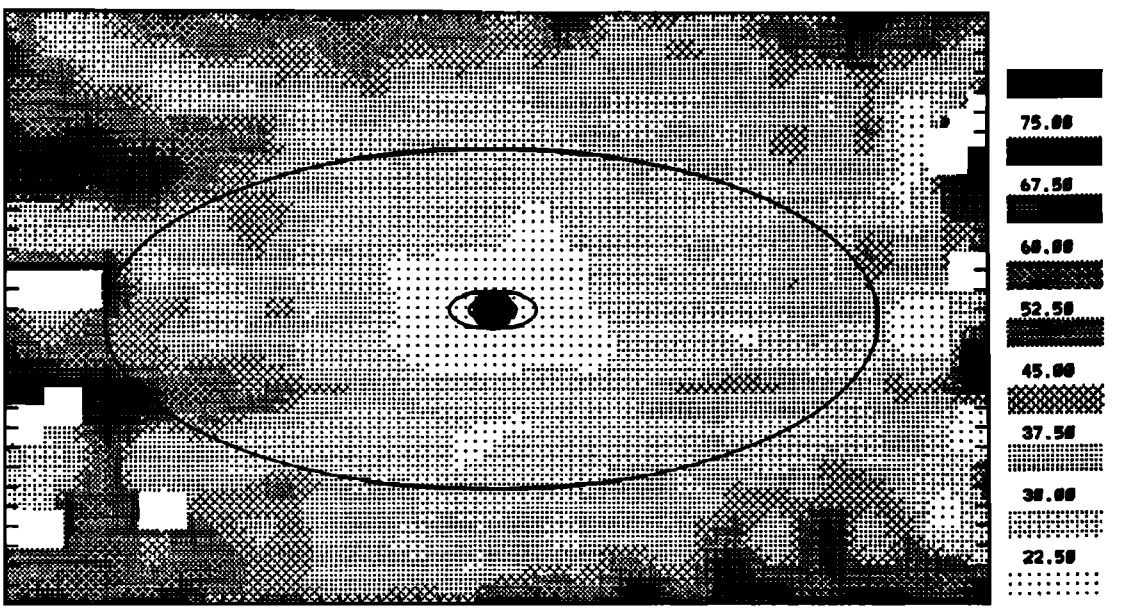

Fig. 1*b*. Statistical 1σ uncertainties corresponding to the data shown in Figure 1*a*. The scale in Rayleighs is given on the right-hand side of the figure.

Figure 5 shows a plot of the brightness as a function of radial distance averaged over the solar and antisolar regions, respectively. A statistically significant peak in emission occurs at 20 R_S in the antisolar region which strongly suggests that Titan acts as a partial source for the atomic hydrogen in the system. The postencounter data were gathered over an interval corresponding to $\approx 1\frac{1}{4}$ Titan orbital periods. The overlap occurred in the antisolar sector and may contribute

to the excess emission observed there. However, emission in the subsolar sector due to a source at Titan may be masked by emission from Saturn coronal hydrogen in the dayside magnetosphere.

Voyager 1 and 2 Preencounter

Previous publications of Voyager UVS results at Saturn describe the region inside of 8 R_S as being void of atomic hydrogen [*Broadfoot et al.*, 1981; *Sandel et al.*, 1982]. This is in conflict with the Voyager 1 postencounter observations outlined above and with the preencounter data described below. Here, we review the preencounter scans conducted by both spacecraft with emphasis on the limitations imposed by observational geometry. We find that the interpretation of a cavity in the H distribution inside 8 R_S is unfounded.

Broadfoot et al. [1981] present the intensity distribution obtained by accumulating several scans conducted by Voyager 1 during the period 1980 DOY 285 to 300 and spacecraft range 730 to 400 R_S [*Broadfoot et al.*, 1981, Figure 7]. A representative scan during this period is illustrated in Figure 6. The observational geometry for these sequences is complicated. Much of the data were obtained in regions partially out of the equatorial plane. Also, because of the significant tilt of the UVS slit with respect to the equatorial plane, these scans cannot discern small scale radial structure in the H distribution. The effective limiting resolution in the equatorial plane is about 9 R_S for the earliest scans improving to about 5 R_S in the latest scans. Any variation in the intensity distribution having spatial scales smaller than this must be statistical in nature. The structure in the *Broadfoot et al.*[1981] plot that suggests the cavity inside 8 R_S is less than this limiting resolution and probably represents statistical fluctuations. Because of the complicated nature of these scans as well as their limited spatial resolution we conclude that this data set is not an optimal choice to investigate spatial structure in the inner Saturn system.

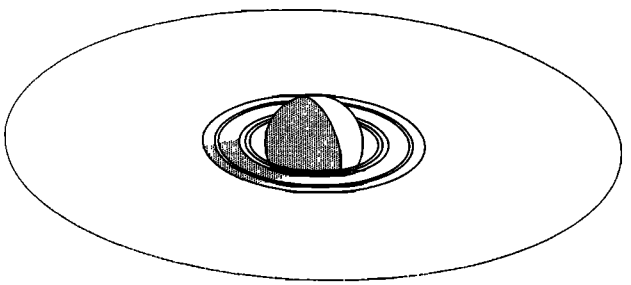

Fig. 2. Close-up of the planetary viewing geometry for the image shown in Figure 1. The shaded areas indicate surfaces in the shadow of the Sun. The bright crescent of the planet has H Ly α brightness $\approx$4000 R. The rings and the orbit of Dione are indicated for reference.

Other preencounter scans conducted by Voyager 1 during the period 1980 DOY 239 to 256 (planet-spacecraft range 1740 to 1370 R_S) suffer less from complicated observing geometry. Representative scans performed during this period are illustrated in Figure 7 where the Saturn system is shown rotated to align the long dimension of the UVS slit with the vertical axis. We have accumulated these scans according to the horizontal position of the slit as depicted in this illustration (the dawnside of the system lies to the left of the planet). The data were accumulated over a time interval of about one Titan orbital period. Times of observations and Voyager flight data system count (FDSC) ranges for these scans are given in Appendix B. The H Ly α intensities are shown in Figure 8. (Note that because of the significant tilt of the orbital plane to the horizontal direction, the elongation points of Titan's orbit lie at $\pm$14 R_S in this plot.) The contribution due to planetary Ly α has been removed by subtracting a scaled version of the H_2 band planetary emissions. This subtraction compounds the statistical errors and is uncertain in absolute magnitude; this is reflected by the large error bars within 3 R_S of the planet in Figure 8. A constant Ly α contribution from the LISM has been subtracted, but no correction has been inserted for the occultation of emissions by the planet. The maximum residual intensity

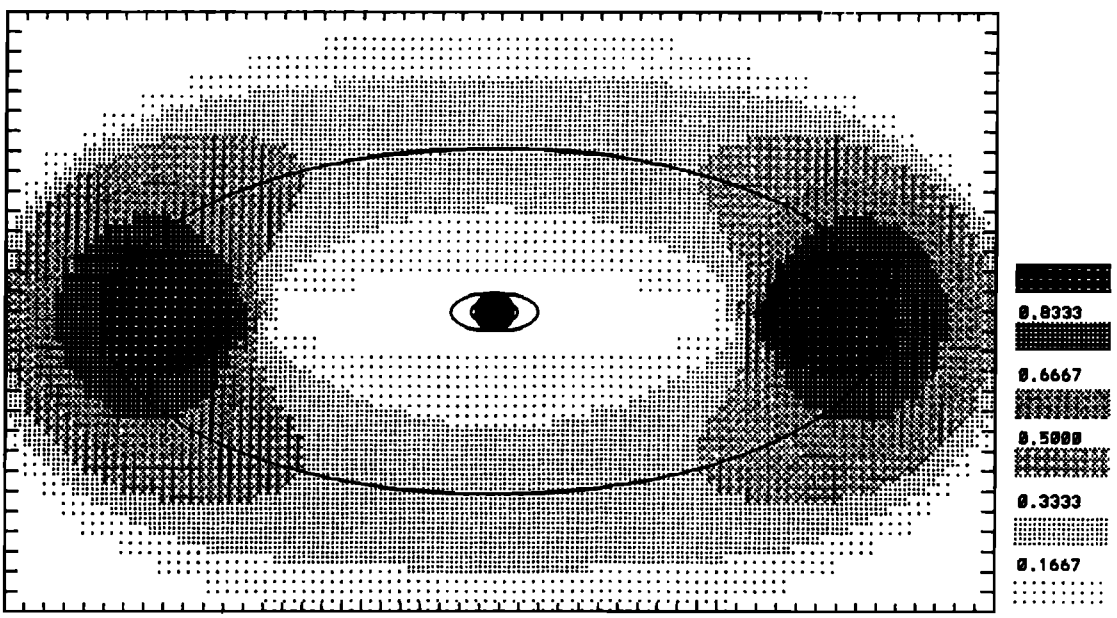

Fig. 3. The predicted distribution of H Ly α emission for the geometry of Figure 1, assuming a uniform torus of minor radius 7 R_S and major radius of 20 R_S. The intensity scale is relative.

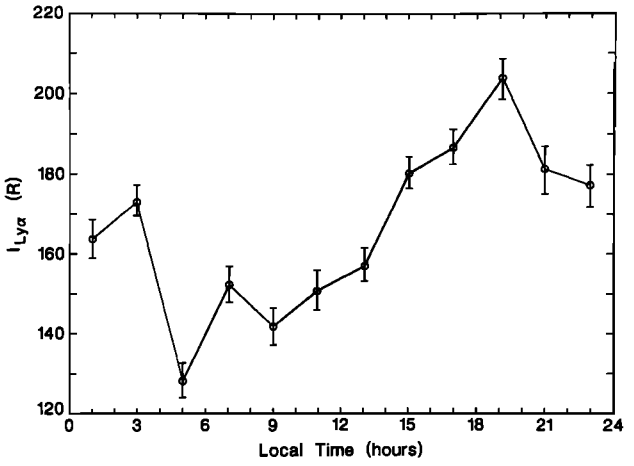

Fig. 4. Mean local time variation of the H Ly α brightness shown in the image given in Figure 1. The data are averaged in 2-hour segments inside 18 R_s.

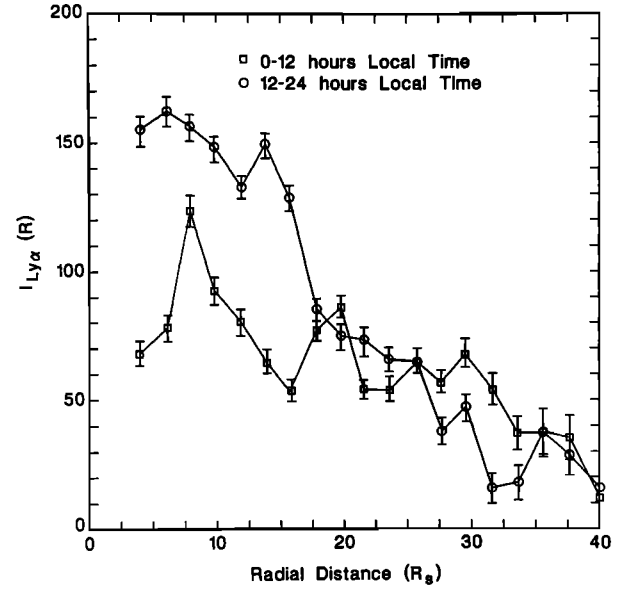

Fig. 5. The distribution of H Ly α emission as a function of radial distance averaged over local time from the data given in Figure 1. A peak in the distribution at $\approx$20 R_S in the 0 to 12-hour data suggests an H source at Titan.

is $\approx$120 R, somewhat lower than the $\approx$150 R reported by *Broadfoot et al.* [1981]. The solar source flux varied by less than 5% during the intervening period. This suggests that the actual emission region does not entirely fill the UVS field of view for the observations illustrated in Figure 7 resulting in a dilution of the aperture averaged intensities. These data show no evidence of a cavity in the inner system nor a significant peak at either ansa of Titan's orbit as one would expect from a Titan-dominated source [see *Smyth*, 1981]. The only readily apparent feature is an excess of emission on the dawnside of the system relative to the duskside.

Voyager 2 preencounter system scans show a similar emission distribution. The representative geometry of scans conducted over the period 1981 DOY 180 to 186 and spacecraft-planet ranges 920 to 820 R_S is shown in Figure 9 with corresponding Ly α intensities plotted in Figure 10. The specific observation times and FDSC ranges are given in Appendix B. Again the scan geometry is relatively simple. (These scans were not accumulated in a tilted coordinate system as were the previous scans because the slit orientation with respect to the equatorial plane changes significantly across the system.) The planetary and LISM emissions have been removed in the same fashion as described above for the Voyager 1 preencounter data. The estimated solar flux during this time is $F_\lambda = 3.1 \times 10^{11}$ Ph cm^{-2} s^{-1} Å^{-1} at 1 AU. This data set appears to be basically consistent with the Voyager 1 data in Figure 8. Excess emission on the dawnside of the planet is apparent and is of the same general relative magnitude as observed by Voyager 1. However, in this case, the observed asymmetry may be due in part to the scan geometry because the instrument slit is falling significantly below the midpoint of Titan's orbital ellipse on the duskside of the system and thus may be excluding relevant emissions. The data show no sign of a peak in the distribution near the ansae of Titan's orbit nor of a cavity in the distribution inside 8 R_S. The variational structure in Figure 10 with characteristic frequencies less than 5 R_S is too frequent to be compatible with the horizontal spatial resolution of the instrument slit (see Figure 9).

The solar flux in H Ly α emission at Voyager 2 preencounter ($F = 3.1 \times 10^{11}$ Ph cm^{-2} s^{-1} at 1 AU) is almost identical to the Voyager 1 preencounter value, based on a prediction using He 10830 Å solar data, normalized to SME satellite measurements in 1982 [*Skinner et al.*, 1988]. The

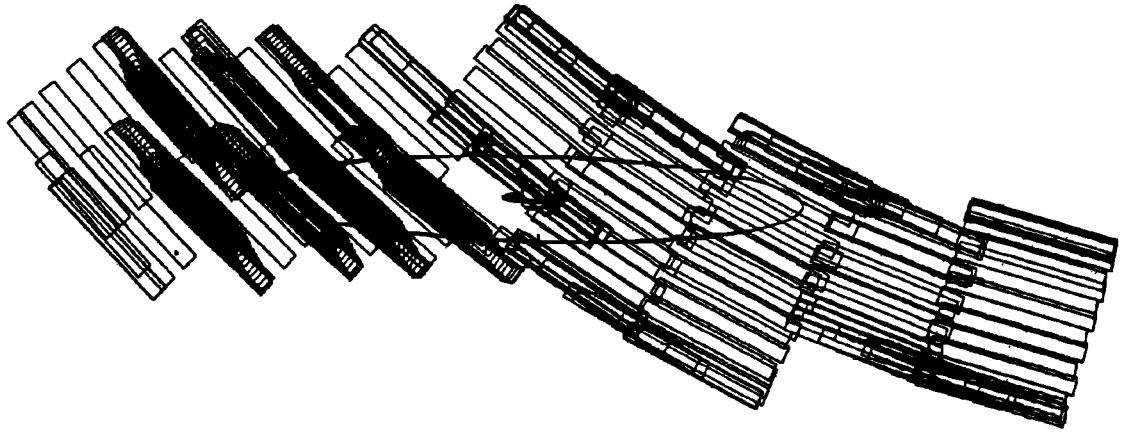

Fig. 6. Representative Voyager 1 preencounter UVS scan conducted during the period 1981 DOY 285 to 300 used to produce Figure 7 of *Broadfoot et al.* [1981]. Saturn and the orbit of Titan are shown to scale. The observations are of a complicated design and much of the data are accumulated with the UVS slit significantly out of the orbital plane.

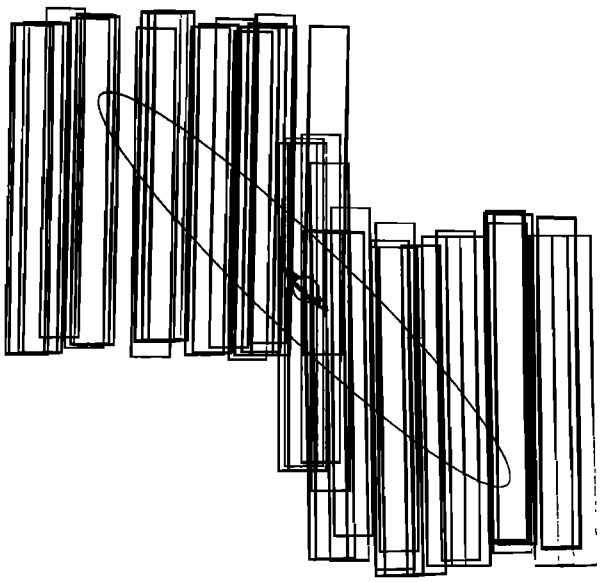

Fig. 7. Representative Voyager 1 preencounter UVS scan conducted during the period 1981 DOY 239 to 256 accumulated to produce the H Ly α intensities in Figure 8. The Saturn system is illustrated rotated to align the vertical direction with the long dimension of the UVS slit.

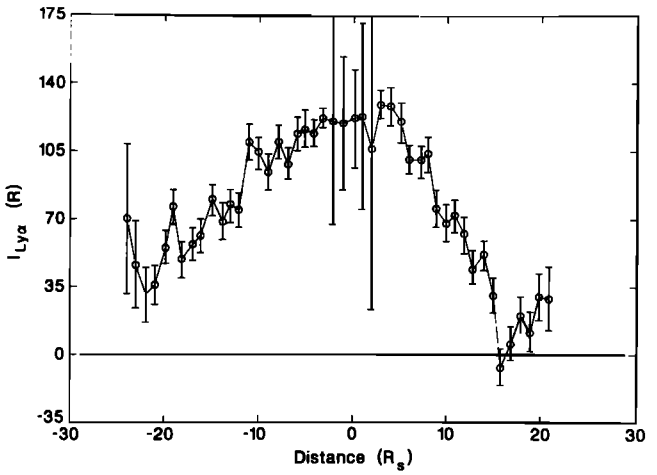

Fig. 8. The H Ly α intensities obtained by summing the scans conducted by Voyager 1 of the form illustrated in Figure 7 (see Appendix B for specific times of observation). Contributions due to the Saturn sunlit atmosphere have been removed using scaled H_2 band planetary intensities. A constant LISM background has also been subtracted.

emission brightness from the left side of Figure 10 (dawnside of the planet) is $\approx$160 R at 10 R_S, essentially the same value as the Voyager 1 preencounter result [*Broadfoot et al.*, 1981]. Evidently the atomic hydrogen abundance in the magnetosphere did not change significantly in the 1-year interval between Voyager encounters.

Discussion

The H distribution defined by the data shown in Figures 1, 4, 5, 8, and 10 is distinctly different from the characteristics derived in earlier research. The brightest regions measured by both spacecraft are within a few R_S of the planet suggesting that the dominant source is at or near Saturn. A contribution from Titan is seen only in the antisolar region of the system. The preencounter scans show a preponderance of emission on the dawnside of the system whereas the postencounter mosaic data show more emission on the duskside. To reconcile this, one may invoke one of the following arguments: (1) The Voyager 1 postencounter image suffers from poor signal-to-noise in the outer regions of the system and the apparent duskside excess may be an artifact of poor statistics and/or inaccurate background removal, or (2) the actual distribution has a complex three-dimensional morphology which yields a brightness distribution highly dependent upon viewer orientation. We discount the first possibility on the ground that the weaker outer region (>22 R_S) shows uniformity in local time after subtraction of the LISM background. It is the brighter inner region that shows local time variability. A background differing from the *Ajello et al.* [1987] model would produce severe nonuniformity in the outer region before the inner region distribution would be significantly affected. The spatial morphology of an H distribution yielding such radically different preencounter and postencounter intensity distributions cannot be simple; taken together, these data sets exclude toroidal or otherwise axially symmetric distributions of H in Saturn's magnetosphere. Given the observed morphology, the Saturn dayside atmosphere appears to be the only reasonable source consistent with the local time variation.

The assumptions made by *Shemansky and Smith* [1982] in suggesting that Saturn was a major source were based on a preliminary analysis of the Voyager 1 data reported by *Broadfoot et al.* [1981]. The latter work inferred the presence of a cavity in the atomic hydrogen distribution in the region inside 8 R_S. Under these circumstances it was necessary to assume that the magnetospheric hydrogen was mainly in stable satellite orbits, allowing the formation of a cavity region through shortened lifetimes in the higher plasma density inside 8 R_S. *Shemansky and Smith* [1982], in suggesting that Saturn was a major source of the magnetospheric hydrogen, simply argued that given the calculated source flux, the major portion of the cloud must be formed of satellite particles collisionally produced from ballistic and escaping atoms.

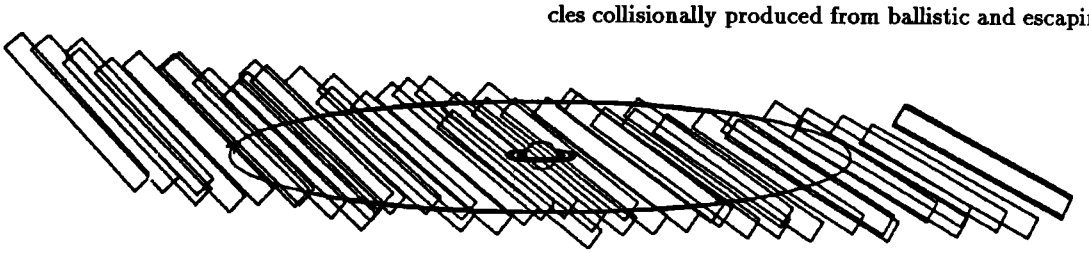

Fig. 9. Representative Voyager 2 preencounter UVS scan conducted during the period 1980 DOY 180 to 186 accumulated to produce H Ly α intensities shown in Figure 5.

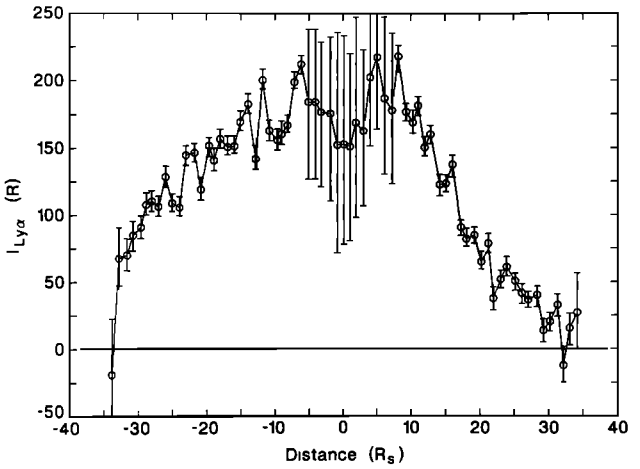

Fig. 10. The H Ly α emission obtained by accumulating scans conducted by Voyager 2 of the form illustrated in Figure 9 (see Appendix B for specific times of observation). Contributions due to planetary and LISM emissions have been removed.

The source distribution in this scenario would be masked by a relatively populous pool of longer-lived satellite atoms [*Shemansky and Smith*, 1986]. However, *Hilton and Hunten* [1988] using a more detailed Monte Carlo calculation including collisional effects, concluded that the production of satellite atoms is a very inefficient process delicately dependent on the source particle energy. This outcome is not entirely clear because the *Hilton and Hunten* [1988] calculations were based on a billiard ball collisional model, which does not include the possibly significant effects of collisions in which electron spins are opposed. A more accurate description of the differential momentum transfer cross sections should be explored. In any case, *Hilton and Hunten* [1988] needed to include a rather large source at Saturn to match the observed distributions, particularly out of the orbital plane. Their required source rate tends to be incompatible with the presence of a cavity inside 8 R_S as interpreted by Broadfoot et al. [1981]. The results presented here indicate that in fact there is a substantial population of H extending into the planetary atmosphere, with densities as high as [H] $\approx$ 100 cm^{-3} between 2 and 10 R_S.

Three facts based on the present results point to Saturn as the major source of the cloud: 1) The radial distribution extends uniformly into the planetary atmosphere. 2) The distinct nonuniformity (Figures 1*a* and 4) of the gas in local time indicates that the source is also nonuniform in local time. The lifetime of hydrogen atoms in the inner magnetosphere has a minimum value of $\tau \approx 100$ days against charge exchange and electron ionization which is much longer than either Saturn's rotational period or Titan's orbital period. A steady source from Titan or the entire Saturn atmosphere should therefore produce an axially symmetric distribution because the atoms would have adequate time to fill the entire azimuthal region. An observed nonuniform distribution either means the source is nonuniform in local time or implies a much shorter H lifetime caused by a physical process other than charge exchange and electron ionization. We believe the former case to be more likely and consider the most viable source region the sunlit Saturn atmosphere. In this case, the observed distribution would be a reflection of an ensemble of exobase atoms on ballistic trajectories passing through the observed volume. H_2 dissociation, probably associated with the H_2 band electroglow phenomenon, could provide adequately energetic H fragments. (3) The abundance of the gas perpendicular to the orbital plane is roughly comparable to the abundance parallel to the plane on the duskside of the system in the region inside $\approx$10 R_S. This characteristic cannot be explained with a source located at Titan's orbit (compare Figures 1*a* and 3; see, for example, *Hilton and Hunten* [1988]). The principal atomic source must therefore be located on Saturn or in the ring system. Saturn's rings have been considered previously as a source of hydrogen and oxygen in the system, stemming from Pioneer and Voyager spacecraft observations of atomic hydrogen in the near-ring vicinity [see *Ip*, 1984, and references therein]. However, a postulated source at the rings has prohibitively serious problems as an explanation for the observed distribution. The source at the rings would necessarily be through photosputtering in order to explain the local time characteristic. The relative constancy of the hydrogen cloud since detection by *Weiser et al.* [1977] is basically incompatible with the factor of $\approx$10 variation in the photosputtering source rate [*Ip*, 1984]. Moreover, loss rates for atomic hydrogen produced in the rings are substantially greater than for the oxygen generated in the same process (Saturn is a major sink for a ring source of hydrogen). Attempts to produce a hydrogen corona from the ring source have ended in the production of prohibitively large amounts of oxygen (W. H. Smyth, private communication, 1987). Finally, source rates for the production of hydrogen from the rings by photosputtering ($\approx 10^{27}$ atoms s^{-1}; *Ip* [1984]) are 2 or 3 orders of magnitude too low for the requirements of the current observations.

The Saturn Source

On the basis of the above considerations, Saturn appears to be the most viable source for both the atomic hydrogen population observed generally inside Titan's orbit. The generation of dissociated atoms in the electroglow in the sunlit atmosphere naturally provides an explanation for the nonuniformity in the local time distribution. The excitation mechanisms are necessarily confined to electron reactions in the vicinity of and above the exobase. Photodissociation cannot play a role because the rates are not of the required magnitude (*D. E. Shemansky*, unpublished manuscript, 1989) and because the bulk of production occurs several scale heights below the exobase. However, as we have pointed out above, the electron impact source rates calculated by *Shemansky and Smith* [1982, 1986] are inadequate to provide the flux required to explain the observed local time variation. The *Shemansky and Smith* [1986] calculation based on the observed H_2 band electroglow emission, interpreted as being produced by electrons with an effective temperature of 30 eV, predicted a total source rate of 3×10^{29} atoms s^{-1} [see *Smith et al.*, 1982]. The calculated rates are based on estimates for the reactions shown in Table 1, with the exception of the dissociative attachment process (see reaction (R14), Table 1). Table 2 shows a rough description of fragment energy ranges for selected electron excitation energies. Roughly 15% of the atomic products are above the escape energy for Saturn. The triplet states of H_2 tend to produce atoms efficiently with energies near 3 eV, the required energy to encounter the rings. The application of a crude approximation to the energy distribution by *Shemansky and Smith* [1986], with the *Smith et al.* [1982] total flux, required most of the H atoms to be in satellite orbits in or-

TABLE 1. Hydrogen Dissociation Reactions

Reaction	Reactants	→ Products	Subsequent Processes
R2*a*	$e + H_2$	$\rightarrow H(n\ell) + H(1s) + e$	
R2*b*		$\rightarrow H(2p) + H(2s) + e$	
R5		$\rightarrow H(n\ell) + H^-$	
R6		$\rightarrow H(1s) + H^+ + 2e$	
R3*a*		$\rightarrow H_2(B) + e$	$H_2(B) \rightarrow H_2(X) + h\nu$; $H_2(X) \rightarrow 2H(1s)$
R3*b*		$\rightarrow H_2(D) + e$	$H_2(D) \rightarrow H(2s) + H(1s)$
R3*c*		$\rightarrow H_2(B') + e$	$H_2(B') \rightarrow H(2s) + H(1s)$
R3*d*		$\rightarrow H_2(B'') + e$	$H_2(B'') \rightarrow H(2s) + H(1s)$
R7		$\rightarrow H_2(a,b,c,e,d,) + e$	
R8		$\rightarrow H_2(c) + e$	$H_2(c) + H_2(X) \rightarrow H_2(a) + H_2(X)$
R9		$\rightarrow H_2(a,c,e,d) + e$	$H_2(a,c,e,d) \rightarrow H_2(b) + h\nu$
R10		$\rightarrow H_2(b) + e$	$H_2(b) \rightarrow 2H(1s)$
R11		$\rightarrow H_2^+ + e$	$H_2^+ \rightarrow H(n\ell) + H^+$
R12		$\rightarrow 2H^+ + 2e$	
R13		$\rightarrow H(n\ell) + H(1s)$	
R14		$\rightarrow H_2^-(a,b,c)$	$H_2^-(a,b,c) \rightarrow 2H(1s) + e$
R15	$e + H_3^+$	$\rightarrow H_2(X) + H(n\ell)$	
R16		$\rightarrow 3H(1s)$	

TABLE 2. Dissociation of H_2 by Electron Impact

Process	Fragment Energy[a] eV			$\sigma(10^{-17}$ cm^2) 15[b]	20[b]	50[b]	100[b]
(1) $H_2(B) \rightarrow H_2(X) \rightarrow 2H(1s)$	0.04	–	1.	0.48	1.38	2.39	2.04
(2) H(2p) + H(1s)	2.	–	8.	0.13	1.30	2.34	2.36
(3) H(2s) + H(1s) predissociation	0.16	–	1.	0.04	0.65	1.41	1.24
(4) H(2s) + H(2p) dissociation	2.8	–	12.	...	0.14	0.16	...
(5) H(3ℓ) + H(1s) predissociation	0.33[c]	and	0.42[c]	...	...	...	...
(6) H(3ℓ) + H(1s) dissociation	4.7	–	8.7	...	0.056	0.18	0.19
(7) H(nℓ), n>7 dissociation	2.8	–	12.	...	0.021	0.024	...
(8) H^+ + H(1s) dissociation	6.	–	11.	...	0.28	0.55	...
(9) $H_2(b) \rightarrow 2H(1s)$ dissociation	2.	–	7.	18.	17.	1.75	0.009
$H_2(a) \rightarrow H_2$ (b)							
$H_2(c) \rightarrow H_2$ (a)							
$H_2(e) \rightarrow H_2$ (a)							
$H_2(d) \rightarrow H_2$ (a)							
TOTAL	...		...	18.7	20.4	8.5	6.6
H(nℓ) Yield > 3 eV	...		...	≈0.6	≈0.6	0.35	0.41
H(nℓ) Yield > 5 eV	...		...	≈0.2	≈0.2	0.18	0.20

[a]Approximate fragment energy range. The directionally dependent H escape energy from Saturn's exobase is 5.7–6.3 eV; 2–3 eV atoms will populate the rings and >4.9 eV atoms will populate the >8 R_S region.

[b]Electron impact energy (eV).

[c]Fragments produced at two discrete energies.

der to account for the observed gas. The source particles in ballistic and escaping orbits calculated by *Shemansky and Smith* [1986] accounted for only 20–25% of the total population of the gas. The current observations require that at least half of the population is in nonstable orbits. The required flux must then be roughly 3 times the value given by *Shemansky and Smith* [1986] or $\approx 10^{30}$ atoms s^{-1}. The difference between the calculated and required values goes well beyond the uncertainties in cross sections for the known dissociative reactions. The energy distribution in the source is roughly estimated but is not expected to account for the discrepancy. The recently measured excitation attachment cross section (*J. M. Ajello et al*, unpublished manuscript, 1989) suggests that a contribution from dissociative attachment ((R14), Table 1) may provide an increased rate but not sufficient to make up the factor of 3 deficiency with observation. Given the present state of understanding of hydrogen reactions and absolute quantities, it appears unlikely that a straightforward translation of H_2 band intensities into atomic hydrogen fluxes from the top of the atmosphere would be in error by more than ≈40%. But the relationship between EUV emission and dissociation rates is sensitive to electron temperature. The efficiency of dissociation by electrons relative to production of EUV radiation rises rapidly with decreasing electron temperature below $T_e \approx 30$ eV [see *Shemansky*, 1985]. However, the character of the EUV emission changes at low electron temperatures and the signature of electrons at temperatures $T_e < 30$ eV does not appear in Saturn spectra (*D. E. Shemansky*, unpublished manuscript, 1989). The analysis based on a single electron temperature is consistent with the observed spectrum and therefore does not allow flexibility in the estimated dissociation rate. However, if electric fields are involved in the excitation process, a single electron temperature may not be a good representation of energy distribution. A multitemperature electron distribution at different altitudes could possibly provide the

required rates, but detailed calculations are necessary to explore the range of parameters allowing compatibility with the observed spectrum.

The nonuniform distribution in local time appears to be qualitatively compatible with an atmospheric source on the sunlit hemisphere. Ballistic flight times for atomic hydrogen would be typically a few hours. The 10-hour rotation period would then tend to provide a bias toward the duskside of the system especially within 10 R_S of the planet. In addition, there are no strong observational constraints on the H source distribution over local time on the sunlit exobase; a nonuniform source could also generate a bias toward the dusk sector. A dusk sector excess is generally consistent with the Voyager 1 postencounter observations. But the preencounter observations performed by both spacecraft show brighter signals on the dawnside of the planet. These data sets may be reconciled if the distribution has a complex three-dimensional morphology that yields larger column densities on the dawnside from the preencounter perspectives and on the duskside from the Voyager 1 postencounter view. For instance, one speculative H distribution that is consistent with both data sets is one where the dawnside distribution extends greater distances from the planet but is confined much more to the orbital plane than on the duskside. From the preencounter perspective the dawnside excess would appear because of the greater radial extent of the dawnside cloud which would increase pathlengths and column densities. However, from the postencounter perspective, if the dawnside H distribution were significantly more confined to the orbital plane than on the duskside, the dawnside column densities would be lower, resulting in stronger emission from the duskside. We do not claim that this speculative H distribution actually exists; its purpose here is to illustrate that the preencounter and postencounter UVS H Ly α observations taken together suggest an H distribution with complex spatial morphology. The spatial structure of the actual H distribution should depend delicately on the H kinetic energy distribution at the Saturn source [see *Hilton and Hunten*, 1988].

Plasma Dynamics in the Inner Magnetosphere

The plasma in the magnetosphere is seriously affected by the presence of neutrals. The plasma content of the Saturn magnetosphere has been determined mainly by the in situ measurements of the Voyager Plasma Science experiment (PLS) [*Bridge et al.*, 1981, 1982]. Both protons and heavy ions were detected. The heavy ions, initially identified as O^+, could not be readily distinguished from ions with similar mass-per-charge ratios such as N^+, OH^+, and H_2O^+. Multiply ionized species near the mass per charge of O^{++} were not detected and must be less than 10% of the total ion population. The plasma environment has been modeled by *Richardson and Sittler* [1990] using the Voyager PLS experimental data. Two populations of electrons are consistent with the data: a suprathermal population with mixing ratio 1–2% and a cold component with a significantly lower temperature than the ions, $T_i/T_{ec} \approx 10$. Our estimate of H density is ≈ 100 cm^{-3} in the $r < 8$ R_S region. *Richardson and Eviatar* [1987] on the basis of model calculations have argued against the presence of atomic hydrogen in amounts [H] > 2 cm^{-3} in the region $r < 8$ R_S. If the H density greatly exceeds this value, they argue that the O^+, believed to be present as the dominant ion in the plasma sheet [see *Richardson and Sittler*, 1990], would be rapidly removed by charge exchange. This conclusion was based on two assumptions: that the source rate of the heavy ions is very limited and that the heavy ion is correctly identified as O^+. Two more recent considerations have altered this scenario by suggesting (1) that the source rate may be very much larger than the *Eviatar* [1984] original estimate [see *Pospieszalska and Johnson*, 1989; *Johnson et al.*, 1989], and (2) that the major ion may be H_2O^+ rather than O^+ [*Eviatar and Richardson*, 1990]. *Barbosa* [1990] has recently discussed conditions in the magnetosphere, arguing that diffusion plays a significant role in determining plasma conditions. We also argue that diffusion must be significantly fast but for a very different reason, and we arrive at different conclusions, as discussed below.

We introduce two additional considerations here in regard to the basic plasma properties. First, the energy budget must be examined quantitatively to determine the sink required to maintain the cold electron population against coulomb heating. We conclude below that cooling of the electrons cannot be accommodated by the assumed O^+ alone. The cooling medium for the cold electrons in our view has therefore not been identified with observed species. Second, we argue that diffusion must play a significant role in controlling conditions in the plasma in order to explain the basic observed plasma properties as derived by *Richardson and Sittler* [1990]. The two points are in fact linked together, since the energy budget depends on diffusive loss rate in an internally consistent calculation. In our calculations described below, the diffusive loss rate is determined essentially by the requirement of a balanced energy budget. *Richardson et al.* [1986] have considered the physical chemistry of the plasma in the inner magnetosphere, but do not examine the energy budget, and utilize a very long diffusive loss time such that diffusion plays no role in the dynamics of the system. *Barbosa* [1990] argues that diffusion plays a significant role, but the plasma energy budget as in the case of *Richardson et al.* [1986] is not considered in his model. The intricacies relating to the plasma sheet are illustrated by considering the properties at a single radial location, $L = 5.5$. The basic physical characteristics of the gas at this location appear to be generally applicable throughout the equatorial plane outside the ring region. We present the basis for the argument briefly below, with the understanding that the processes must be considered in more detail to obtain a more definite resolution.

Heavy ions in this region detected by the Voyager PLS have been interpreted as O^+ [*Bridge et al.*, 1981]. In this interpretation, typical densities at 4.5 R_S (L = 5.5) in the equator are $[H^+] \approx 3$ cm^{-3}, $[O^+] \approx 30$ cm^{-3}, $[e] \approx 33$ cm^{-3} [*Richardson and Sittler*, 1990] . Table 3 shows the plasma parameters modeled by *Richardson and Sittler* [1990] , in which it is assumed that the major heavy ion is O^+. This species is lost mainly by the following reactions:

$$O^+ + e \rightarrow O^{++} + 2e \quad \text{(R17)}$$

$$O^+ + O \rightarrow O + O^+ \quad \text{(R18)}$$

$$O^+ + H \rightarrow H^+ + O \quad \text{(R19)}$$

$$O^+ \longrightarrow diffusion. \quad \text{(R20)}$$

Although (R18) does not represent a net loss of O^+, it does indicate a loss of mass from the volume that must be replaced by the source. Because the majority of electrons are cold with $T_{ec} \approx 4$ eV at $L = 5.5$, physical chemistry rates

TABLE 3. Plasma Parameters at the Saturn Magnetic Equator, L=5.5

Species	Density, cm^{-3}	Temperature, eV
e_c	31.7	4.0
e_h	0.4	130.0
O^+	29.0	90.0
H^+	2.7	15.0

From *Richardson and Sittler*[1990].

preferentially reduce molecules to neutral dissociation products. The hot electron population detected by the Voyager PLS experiment [*Richardson and Sittler*, 1990] also plays an important role in controlling conditions in the plasma. Given the measured electron environment and the reactions identified in Table 4, we find that the source particles for the formation of O^+ must be dominated by atomic oxygen, mainly in order to reproduce the observed ratio of heavy to light ions. The loss of atomic oxygen from the volume is controlled by the reactions,

$$O + e \rightarrow O^+ + 2e \quad \text{(R21)}$$

$$O + O^+ \rightarrow O^+ + O \quad \text{(R18)}$$

$$O + H^+ \rightarrow O^+ + H \quad \text{(R22)}$$

$$O + h\nu \rightarrow O^+ + e. \quad \text{(R23)}$$

Of this set, reactions (R21) and (R18) define the loss as shown by the rates given in Table 4. The equilibrated state of the gas in the model depends principally on the assumed relative rates of injection of the neutral species and ion diffusive loss probability. It is beneficial at this point to discuss basic differences in rate processes used here and those of *Richardson et al.* [1986] .

The principal differences in rate processes utilized by *Richardson et al.* [1986] and those contained in Table 4 are the direct electron impact dissociation reactions of the molecular species. These reactions are not included by *Richardson*

TABLE 4. Saturn Magnetosphere Processes

	Reaction	k_{ij} 10^{-9} cm^3 s^{-1}	$[N_j]$ cm^{-3}	P_i 10^{-8} s^{-1}	τ_i days
R17	$O^+ + e \rightarrow O^{++} + 2e$	0.33	31.7	1.03	1120.
R18	$O^+ + O \rightarrow O + O^+$	10.5	414.	435.	2.7
R19	$O^+ + H \rightarrow H^+ + O$	7.0	100.	70.	16.5
R36	$O^+ + O_2 \rightarrow O_2^+ + O$	...	...	...	...
R54	$O^+ + OH \rightarrow OH^+ + O$	...	36.	...	...
R55	$O^+ + OH \rightarrow H^+ + O_2$	...	36.	...	...
R20	O^+ diffusion[a]	...	...	30.	39.
	O^+ total loss[b]	...	...	561.	2.1
R21	$O + e \rightarrow O^+ + 2e$	1.4	31.7	4.44	261.
R22	$O + H^+ \rightarrow O^+ + H$	7.0	2.7	1.89	612.
R18	$O + O^+ \rightarrow O + O^+$	9.9	29.0	28.7	40.3
R23	$O + h\nu \rightarrow O^+ + e$	...	...	0.23	5030.
	O total loss[b]	...	...	35.3	32.8
R24	$H_2^+ + e \rightarrow H + H$	31.0	31.7	98.3	11.8
R25	H_2^+ diffusion[a]	...	...	240.	4.8
	H_2^+ total loss[b]	...	...	338.	3.4
R26	$H_2 + e \rightarrow H_2^+ + 2e$	0.95	31.7	3.0	383.
R27	$H_2 + e \rightarrow H + H + e$	2.83	31.7	9.0	129.
R28	$H_2 + h\nu \rightarrow H + H$	...	...	0.34	3400.
R29	$H_2 + h\nu \rightarrow H_2^+ + e$	...	...	0.054	21000.
R30	$H_2 + h\nu \rightarrow H + H^+ + e$	...	...	0.010	$1.\times10^5$
	H_2 total loss[b]	...	...	12.4	93.3
R31	$O_2^+ + e \rightarrow O^+ + pd$[c]	21.7	31.7	68.8	16.8
R32	$O_2^+ + e \rightarrow O + O$	15.3	31.7	48.5	24.
R33	O_2^+ diffusion[a]	...	...	15.0	77.
	O_2^+ total loss[b]	...	...	132.	8.8
R34	$O_2 + e \rightarrow O + O + e$	21.5	31.7	68.2	17.0
R35	$O_2 + e \rightarrow (O + O^+)$ and $(O_2^+) + 2e$	2.9	31.7	9.1	127.
R36	$O_2 + O^+ \rightarrow O_2^+ + O$	2.1	29.0	6.09	190.
R37	$O_2 + OH^+ \rightarrow OH + O_2^+$	0.20	...	...	...
R38	$O_2 + h\nu \rightarrow O_2^+ + e$	...	...	0.56	2070.
R39	$O_2 + h\nu \rightarrow O + O$	...	...	6.60	175.
R40	$O_2 + h\nu \rightarrow O^+ + O + e$	...	...	0.058	20000.
	O_2 total loss[b]	...	...	90.6	12.8
R41	$OH^+ + e \rightarrow H + O$	6.8	31.7	21.6	53.7
R42	$OH^+ + e \rightarrow H^+ + O + e$	36.0	31.7	114.	10.1
R43	$OH^+ + e \rightarrow H + O^+ + e$	36.0	31.7	114.	10.1
R44	$OH^+ + H_2O \rightarrow O + H_3O^+$	12.5	18.	22.8	50.9
R45	$OH^+ + H_2O \rightarrow OH + H_2O^+$	14.0	18.	25.5	45.4
R37	$OH^+ + O_2 \rightarrow OH + O_2^+$	0.20	...	...	...
R46	OH^+ diffusion[a]	...	...	28.2	41.0
	OH^+ total loss[b]	...	...	326.	3.6

et al. [1986] . Two other differences leading to significantly divergent conclusions are the neglect of the process ionizing O^+ to produce O^{++} (R17) by *Richardson et al.* [1986] and their utilization of a very long ion diffusive loss time. We find that given the same conditions, the results obtained by *Richardson et al.* [1986] can be reproduced in our calculations to a satisfactory approximation. The plasma model based on the rates of Table 4 is obtained using the methodology described by *Shemansky* [1988]. The calculation is based on a volumetric average, and source injection rates are uniform in the plasma volume. The source rates of the neutral species required to maintain the system in steady state are dictated by the aggregate loss processes in the plasma. The neutral species densities in the gas are therefore determined internally to the model calculation, dictated by physical chemistry, the imposed diffusive loss time, and the electron parameters fixed by the Voyager PLS experiment.

The partitioning of species for the conditions selected by *Richardson et al.* [1986] are given in lower half Table 5, calculated using the methodology described briefly above. These results are characterized by small neutral species populations because of assumed very long diffusive loss times (τ_d = 35 years). The partitioning of source species in this case does not provide the relative light and heavy ion populations obtained from the observations. More importantly, the results for this case in Table 5 show that most of the O^+ has been converted to O^{++}. The crucial point here is that the Voyager PLS experiment rules out the presence of measurable O^{++}, and the suppression of this species can be obtained only by increasing the diffusive loss probability. We note that *Frank et al.*[1980] argued that the Pioneer 11 results were more compatible with the presence of O^{++} than O^+, based on best fits to ion velocity distributions. However, the *Frank et al.*[1980] analysis also pointed to He^+ as

TABLE 4. (continued)

Reaction		$k_{i,j}$ 10^{-9} cm^3 s^{-1}	$[N_j]$ cm^{-3}	P_i 10^{-8} s^{-1}	τ_i days
R47	$OH + e \rightarrow O + H + e$	1.09	31.7	3.45	335.
R48	$OH + e \rightarrow OH^+ + 2e$	2.17	31.7	6.88	168.
R49	$OH + e \rightarrow O^+ + H + 2e$	0.77	31.7	2.45	472.
R50	$OH + e \rightarrow H^+ + O + 2e$	0.36	31.7	1.13	1020.
R51	$OH + h\nu \rightarrow OH^+ + e$	...	...	0.37	3100.
R52	$OH + h\nu \rightarrow O + H$	...	...	19.1	61.0
R53	$OH + H^+ \rightarrow OH^+ + H$	0.30	2.7	0.081	14000.
R54	$OH + O^+ \rightarrow OH^+ + O$	0.30	29.0	0.87	1330.
R55	$OH + O^+ \rightarrow H^+ + O_2$	0.12	29.0	0.35	3300.
	OH total loss[b]	...	...	34.7	33.4
R56	$H_2O^+ + e \rightarrow OH + H$	7.4	31.7	23.3	49.6
R57	$H_2O^+ + e \rightarrow OH^+ + H + e$	31.8	31.7	101.	11.5
R58	$H_2O^+ + e \rightarrow OH + H^+ + e$	8.05	31.7	25.5	45.4
R59	H_2O^+ diffusion[a]	...	...	26.7	43.4
	H_2O^+ total loss[b]	...	...	176.	6.6
R60	$H_2O + e \rightarrow H_2O^+ + 2e$	1.6	31.7	5.07	228.
R61	$H_2O + e \rightarrow OH^+ + H + 2e$	0.55	31.7	1.73	669.
R62	$H_2O + e \rightarrow H^+ + pd$[c]	0.34	31.7	1.09	1060.
R63	$H_2O + e \rightarrow O^+ + pd$[c]	0.067	31.7	0.21	5450.
R64	$H_2O + e \rightarrow H + OH + e$	17.6	31.7	55.6	20.8
R65	$H_2O + H^+ \rightarrow H_2O^+ + H$	8.8	2.7	2.38	487.
R44	$H_2O + OH^+ \rightarrow O + H_3O^+$	12.5	...	...	...
R45	$H_2O + OH^+ \rightarrow OH + H_2O^+$	14.0	...	...	...
R67	$H_2O + h\nu \rightarrow OH + H$	...	...	10.6	109.
R68	$H_2O + h\nu \rightarrow H_2 + O$	...	...	1.49	777.
R69	$H_2O + h\nu \rightarrow H_2O^+ + e$	...	...	0.37	3130.
R70	$H_2O + h\nu \rightarrow OH^+ + H + e$	...	...	0.061	19000.
R71	$H_2O + h\nu \rightarrow O^+ + H_2 + e$	...	...	0.006	$2.\times10^5$
	H_2O total loss[b]	...	...	78.6	14.7
R72	$H_3O^+ + e \rightarrow OH^+ + H_2 + e$	...	...	...	...
R73	$H_3O^+ + e \rightarrow OH + H_2$	...	36.	...	...
R74	H_3O^+ diffusion[a]	...	...	25.3	45.8
	H_3O^+ total loss[b]	...	...	25.3	45.8
R75	$N^+ + e \rightarrow N^{++} + 2e$	0.43	31.7	1.38	841.
R76	$N^+ + N \rightarrow N + N^+$	10.	...	...	...
R77	$N^+ + H \rightarrow H^+ + N$	1.1	100.	11.	105.
R78	N^+ diffusion[a]	...	...	34.3	34.
	N^+ total loss[b]	...	...	46.6	25.
R79	$N + e \rightarrow N^+ + 2e$	1.72	31.7	5.45	212.
R76	$N + N^+ \rightarrow N^+ + N$	10.	...	...	...
R80	$N + H^+ \rightarrow N^+ + H$	...	2.7	...	...
R81	$N + h\nu \rightarrow N^+ + e$	...	...	0.2	5790.
	N total loss[b]	...	...	5.6	205.

[a]Diffusion rate, $(P_i)_{diff}$, is proportional to species charge/mass ratio.

[b]Minimum total loss rate is tabulated because some loss processes are neglected.

[c]Unknown dissociation product(s).

TABLE 5. Model of Plasma Partitioning 4.5 R_S in the Saturn Magnetosphere

	[O]	[H]	[OH]	[H_2O]	[O^+]	[H^+]	[O^{++}]	[H_2O^+]
			τ_d = 40 days, [n_e] = 31.8 cm^{-3}					
[N][a]	414.	136.	35.5	18.2	24.5	3.29	0.43	1.05
$\dot{N}$[b]	120.	...	...	15.1	...	...	...	...
$\dot{Y}$[c]	2800.	...	...	350.	...	...	...	...
			τ_d = 35 years, [n_e] = 31.8 cm^{-3}					
[N][a]	0.82	0.61	0.02	0.01	2.71	0.59	14.2	0.0004
$\dot{N}$[b]	0.059	...	...	0.0074	...	...	...	...
$\dot{Y}$[c]	1.38	...	...	0.17	...	...	...	...

[a] Number density (cm^{-3}).
[b] Volumetric source rate (10^{-6} $cm^{-3}s^{-1}$).
[c] Total source rate(10^{24} s^{-1}) for torus r = 1 R_S, R = 5.5 R_S.

the dominant low mass per charge ion. We have assumed that the Voyager PLS result is applicable. *Richardson et al.* [1986] neglected the production of O^{++}, leaving O^+ as the terminal ion in their results. The inclusion of dissociative reactions in our calculations relegates molecular ions to the category of minor species under all assumed conditions. If we take the reactions in Table 4 as basically correct, the major heavy ion in the plasma must be atomic. Ion diffusive loss plays no role in the terminal plasma condition calculated by *Richardson et al.* [1986] . The presence of the observed anisotropy ($A \equiv T_\perp/T_\parallel$ - 1) of 5 [*Richardson and Eviatar*, 1988] in the heavy ions would be impossible to reproduce under the conditions imposed by the present rate processes (Table 4) for long diffusive loss times. The rate processes in our calculations therefore produce results incompatible with observation on several counts when the parameters applied by *Richardson et al.* [1986] are implemented. As discussed below, energy balance in the plasma sheet also becomes a serious problem under these conditions.

Table 5 shows the calculated state of the plasma after the application of source conditions and diffusive loss rates necessary to reproduce the basic observational constraints (τ_d = 40 days). A range of heterogenous source partitioning and diffusive loss times will provide satisfactory results, but we do not explore this parameter space here. Assuming the ion diffusive loss rates are proportional to the species charge-to-mass ratio, we find that a large heterogenous source of atomic oxygen is required in order to provide the requisite relative numbers of heavy and light ions. The diffusive loss time is dictated by the necessity to suppress O^{++} to the extent required by observation and to provide an approximate balance in the energy budget. The higher source and loss rates provide basic compatibility with the observed quantity of atomic hydrogen determined in the present analysis. Atomic oxygen is the dominant neutral in the plasma sheet in this scenario, with a density of $\approx$400 cm^{-3}. Given the values in Table 4, the loss of atomic oxygen by symmetric charge exchange and ionization (reactions (R18) and (R21)) requires that the atoms be replaced at a rate of $\approx 10^{-4}$ cm^{-3} s^{-1}. In the volume contained in an assumed torus of 1 R_S minor radius and 4.5 R_S major radius, with volume $V = 2.0 \times 10^{31}$ cm^3, the loss rate of O is $\approx 3 \times 10^{27}$ atoms s^{-1} (Table 5). This rate is 3 orders of magnitude larger than the value estimated by *Eviatar* [1984] and $\approx$30 times larger than the *Johnson et al.* [1989] estimate for ion sputtering of the icy satellite surfaces. Although this rate is substantially larger than the previous estimates, there is an inherent difficulty in translating laboratory surface reactions to icy satellite surfaces, and other possible sources may contribute. We emphasize that the present results are preliminary. Further research in physical chemistry and source processes is required to establish more definitive statements on critical rate processes.

Since O^{++} is observationally limited to 10% of the ion population, diffusive loss rates (reaction (R20)) must be of the order given in Table 4. The diffusive loss rate derived by *Barbosa* [1990] is similar to the value we obtain in Table 5. The *Barbosa* [1990] calculations appear to limit loss rates by adjusting the neutral species content downward in order to limit loss rates to the value established by *Johnson et al.* [1989]. In the present calculations the neutral species content is dictated by physical chemistry and the requirement for approximate balance in the energy budget.

Energy balance in the plasma has not been considered quantitatively in previous work. The cold pool of electrons measured by the PLS instrument must absorb energy from the ions and hot electrons in the volume. The coulomb collisional rates for these processes are given in Table 6. The dominant flow is from the hot electrons, with a total rate of 70×10^{-17} ergs cm^{-3} s^{-1}. The cold electrons lose less than 10% of this source to O^+ and about 28% to atomic hydrogen. The remainder is approximately accounted for by the predicted quantities of atomic oxygen and OH (Table 6). It is therefore not possible to account for the population of cold electrons in the plasma sheet without invoking the presence of substantial numbers of neutral species. The cold electrons in the plasma are heated at a rate representing a 3-day time constant for relaxation upward to an asymptotic 130 eV. The presence of *E* ring particles as discussed by *Hood* [1989], may contribute to electron cooling, but as discussed below, this factor is not likely to be significant. In fact, the particle distribution shows strong radial variations, and the differences in the calculated flow of energy at larger radial locations remain of an order comparable to the values given here for L = 5.5. Although nitrogen has an intrinsically larger radiative cooling efficiency, it is not expected to be present in the inner region in sufficient quantities [*Ip*, 1990] to affect the flow of energy. Nitrogen may play a larger role in the plasma sheet at radial locations beyond $\approx$10 R_S, but discussion of plasma in the outer region is beyond the scope of this paper.

Richardson and Eviatar [1988] have pointed out that the heavy ion pitch angle anisotropy is large with accompanying kinetic energies near the corotation pickup value. They are able to explain the distribution if the ion is a water group molecule, through the short dissociative recombination lifetimes. If the ion is O^+ according to the argument above, the anisotropy cannot be explained in the same way. In this case, the O^+ ion is maintained with high anisotropy and near

TABLE 6. Energy Transport in the Saturn Magnetosphere at L = 5.5

Species		Rate Factors	
Source	Sink	Coefficient 10^{-20} erg cm^3 s^{-1}	Rate 10^{-17} erg cm^{-3} s^{-1}
O^+	e_c	8.0	7.3[a]
e_h	e_c	5030.	63.[b]
Total flow to cold electrons			70.[c]
e_c	O^+[d]	5.8	5.3
e_c	O^+[e]	0.006	...
e_c	N^+[d]	11.	...
e_c	N^+[e]	0.06	...
Total cold electron loss to ions			5.3[c]
e_c	O[d]	2.2	28.[f]
e_c	O[e]	1.1	14.
e_c	OH[d]	1.9	2.2[h]
e_c	OH[e]	6.8	7.5[i]
e_c	N[d]	8.0	0.13[g]
e_c	N[e]	1.4	0.02
e_c	H[d]	4.5	20.[f]
e_c	H[e]	0.87	3.8
Total cold electron loss to neutrals			76.[j]

[a] Coulomb collision transfer [see *Spitzer*, 1962, equations (5)-(31)].

$\tau_{eq} = \frac{5.87 A_e A_i}{[e] Z_e^2 Z_i^2 \ell n \Lambda} \left(\frac{T_e}{A_e} + \frac{T_i}{A_i}\right)^{\frac{3}{2}}$ s; $\frac{dE_i}{dt} = \left(\frac{E_e - E_i}{\tau_{eq}}\right)$ erg s^{-1} ion^{-1};

$\Lambda = \frac{3}{2 \cdot Z_e Z_i e^3} \cdot \left(\frac{k^3 T_e^3}{\pi [e]}\right)^{\frac{1}{2}}$.

[b] The limiting case in which the hot electron rms velocity much exceeds the rms velocity of the field particles [*Spitzer*, 1962, equations (5)-(18), (5)-(28), (5)-(14)].

$t_s = \frac{\bar{v}^3}{A_D}$; $A_D = \frac{8\pi e^4 [e_c] \ell n \Lambda}{m_e^2}$; $\frac{d\bar{E}_e}{dt} = -\frac{2\bar{E}_e}{t_s}$; $\bar{E}_e = \frac{1}{2} \cdot m_e \cdot \bar{v}^2$.

[c] The major heavy ion is assumed to be O^+.

[d] Radiative cooling.

[e] Ionization.

[f] Densities (cm^{-3}) inferred from model calculations given in Table 5; [O] = 414; [H] = 136; [OH] = 36; [H_2O] = 18.

[g] Rough value from *Ip* [1990]; [N] = 0.5 cm^{-3}.

[h] Radiation and dissociation.

[i] Ionization and dissociative ionization.

[j] No attempt has been made to achieve exact equilibrium in flow of energy in the model calculation.

corotation energy by symmetric charge exchange with atomic oxygen, with a lifetime of ≈3 days. Without the presence of large numbers of neutrals generated by high source rates, the O^+ would relax to isotropy and lose its dominance through conversion to O^{++}.

Implied Heating of the Saturn Upper Atmosphere

The large source of atomic hydrogen required by the observed magnetospheric distribution implies that the Saturn atmosphere in the interaction region must be heated by the downward neutral flux component. Recent calculations of thermal deposition rates by the dissociation process (Strobel and Shemansky, unpublished manuscript, 1988) using the *Shemansky and Smith* [1986] source estimates fall short of predicting the measured thermospheric temperature, with an optimistic value T_∞ = 340 K compared to the measured T_∞ = 420 K. However, the increased source rates required by the current observations can provide the required collisional heating. A factor of 2 increase in energy deposition rate would raise the predicted value to T_∞ = 480 K if all of the energy is deposited at the exobase.

SUMMARY AND CONCLUSIONS

The data presented in this article consist of three sets of previously unpublished UVS observations of the Saturn system conducted by both Voyager spacecraft. Voyager 1 postencounter mosaic data obtained when the spacecraft was 26° out of the equatorial plane have been accumulated to produce an image of the H Ly α emission distribution (Figure 1). The distribution shows emission extending from Titan's orbit to the Saturn upper atmosphere, nonuniform in local time in the region inside 18 R_S with a preponderance of emission on the duskside of the system. The Voyager 1 postencounter intensities are comparable to those measured in preencounter sequences obtained with the spacecraft nearly in the equatorial plane implying an H distribution with comparable abundances within and perpendicular to the equatorial plane on the duskside of the system. Excess emission associated with the orbit of Titan is detected in the antisolar region (i.e., 1200 to 2400 LT). The Voyager 1 and 2 preencounter data sets, however, show no peak in emission associated with Titan's orbit (Figures 8 and 10). The preencounter intensities measured by both spacecraft increase monotonically toward the planet. The preencounter scans reveal more emission on the dawnside of the system than the duskside. This may be reconciled with the Voyager 1 postencounter duskside excess if there exists a complex H distribution with significant radial and azimuthal variations. Simple, axially symmetric toroidal or disklike distributions are precluded by the new data sets.

The observed nonuniform emission within 10 R_S of the planet indicates that a substantial fraction of the H population is composed of atoms in ballistic and escaping trajectories from a nonuniform source at Saturn. The required source rate at Saturn is crudely estimated to be 10^{30} atoms s^{-1}. Photoexcitation cannot contribute and the source mechanism is attributed to electron interaction in the vicinity of the exobase and in the exosphere. The required source of atomic hydrogen from the Saturn upper atmosphere can account for the observed thermospheric temperature. The excess emission observed in the antisolar region near 20 R_S implies that Titan is also a significant source of atomic hydrogen and probably dominates in the region outside 18 R_S.

A preliminary examination of the dynamics of the plasma sheet in the inner magnetosphere indicates on several counts that substantial numbers of neutral species must be present. If H_2O chemistry is the source of the heavy ion plasma, the major ion must be O^+ according to our analysis. A relatively short diffusive loss time is then required in order to explain (1) the nondetection of O^{++}, (2) the observed large heavy ion pitch angle anisotropy, (3) the existence of O^+ against charge exchange losses to the significant population of atomic hydrogen, and (4) the existence of the dominant population of cold electrons in the plasma sheet. The density of neutral oxygen atoms in the plasma sheet required to explain the observed heavy ion/light ion population ratio is ≈400 cm^{-3} near 4.5 R_S, for an O^+ diffusive loss time of ≈40 days. The density of OH present is predicted to be ≈40 cm^{-3}. The inferred densities of atomic oxygen and OH would account for most of the energy loss required to maintain the observed pool of cold electrons.

APPENDIX A: VOYAGER 1 UVS SATURN POSTENCOUNTER MOSAIC

This appendix discusses the data reduction and background removal processes used to create Figure 1, which shows the H Ly α emission from the Saturn system as determined from a summation of 18 scans performed by Voyager 1 in the period 1980 DOY 324–343 (6 to 25 days postencounter). These scans were designed to provide complete coverage of the Saturn system within and just beyond the orbit of Titan. Table A1 gives the Voyager 1 spacecraft event times and FDS counts of the sequences used in the summation. The planet-spacecraft range, also given in Table A1, varied from 8.64×10^6 to 3.35×10^7 km.

During the periods given in Table A1, the Voyager UVS obtained 126 hours of total exposure time composed of spectra 3.84 s in duration. These spectra are summed into 1 R_S by 1 R_S integration elements according to the intersection of the UVS central line of sight with the summation plane which is the plane passing through the center of the planet, perpendicular to the planet-spacecraft line. The planet-spacecraft line intersects the orbital plane at an angle of about 26° so the orbit of Titan traces out an ellipse with semimajor and semiminor axes of $\approx$20 R_S and $\approx$8 R_S in the summation plane. Because of the 26° declination, each 1 R_S by 1 R_S square element in the summation plane corresponds to a rectangular element in Titan's orbital plane measuring 1.0 R_S by 2.4 R_S.

TABLE A1. Voyager 1 Saturn Postencounter Mosaic Scan Information, 1980

Onset DOY	Δt hours	Initial FDS Count	Final FDS Count	Planet - s/c Range, km
324.23	6.58	35127:08	35135:21	8.46 (6)[a]
325.11	6.58	35153:33	35161:46	9.81 (7)
326.00	6.58	35179:57	35188:10	1.10 (7)
326.97	6.58	35209:18	35217:31	1.23 (7)
328.85	17.98	35258:33	35281:01	1.48 (7)
330.08	6.31	35302:43	35310:35	1.64 (7)
331.18	6.31	35335:50	35343:42	1.78 (7)
332.17	6.31	35365:21	35373:13	1.91 (7)
333.16	6.31	35395:01	35402:56	2.04 (7)
334.15	6.31	35424:58	35432:50	2.17 (7)
335.15	6.31	35454:53	35462:45	2.31 (7)
336.15	6.31	35484:47	35492:39	2.44 (7)
337.15	6.31	35514:55	35522:47	2.57 (7)
338.17	6.31	35545:27	35553:19	2.70 (7)
339.15	6.31	35574:44	35582:36	2.83 (7)
340.14	6.31	35604:38	35612:30	2.96 (7)
342.14	6.31	35664:27	35672:19	3.22 (7)
343.13	6.31	35694:22	35702:14	3.35 (7)

[a] 8.46 (6) = 8.46×10^6.

Each integration element in the summation plane represents an accumulated Voyager UVS spectrum. After correction for instrumental Fixed Pattern Noise (FPN) [*Broadfoot et al.* 1977] these spectra contain one or more of the following components: (1) UVS "dark counts," (2) galactic ultraviolet background radiation, (3) diffuse stellar ultraviolet continuum, (4) HI 1216 Å , HI 1025 Å and HeI 584 Å lines due to solar photons resonantly scattered from the local interstellar medium (LISM), and (5) emissions from the Saturn system. The first four of these are considered background and, if necessary, subtracted from the data to leave the residual Saturn system emissions. Even though the three resonance lines mentioned above all appear in the spectra, only the H Ly α (1216 Å) line has an adequate signal-to-noise ratio to justify analysis. The UVS dark count spectrum is representative of the particle and radiation noise in the spacecraft environment [*Broadfoot et al.* 1977; *Holberg* 1986]. It is mainly due to a marginal UVS sensitivity to radiation emitted from the radioisotope thermoelectric generators (RTG), the spacecraft nuclear power supply. During planetary encounters the dark counts can vary in rate as well as change in spectral shape due to magnetospheric radiation. For these mosaic scan sequences, however, the spacecraft was far enough from the Saturn magnetosphere to allow a normal correction for radiation background. The Galactic H Ly α background has been shown to be less than 20 R [*Wu et al.* 1981] and any galactic continuum emission lying in the H Ly α channel range is small compared to the LISM scattered H Ly α component [*Holberg* 1986]. We neglect the galactic contribution in H Ly α in the analysis.

Both the stellar ultraviolet continuum radiation lying in the H Ly α channels and the resonantly scattered LISM H Ly α are nontrivial backgrounds and are explicitly removed from the data. LISM H Ly α contamination from the UVS occultation port is also removed. After these subtractions we perform a two-dimensional smoothing and plot the resulting image in Figure 1*a*.

Stellar Continuum Background Removal

The Saturn postencounter trajectory of Voyager 1 curved up and out of the ecliptic plane. The spacecraft-planet pointing changed from a right ascension (α) and declination (δ) (earth mean equatorial, 1950) of 58.2° and -31.5° on 1980 DOY 324 to 58.8° and -32.5° on 1980 DOY 343. During this time the angular projection of the semimajor axis of Titan's orbital ellipse decreased from about 8.2° to 2.0° because of increasing planet-spacecraft range. The stellar flux detected between 950 and 1170 Å is plotted in Figure A1. Notice, the west ansa region as well as the region directly south of the planet are the areas most contaminated by stellar background. For the spectra corresponding to these integration elements we estimated the stellar continuum contribution in the H Ly α channels by correlation with the measured signal between 950 and 1170 Å . For the most contaminated spectra, the subtracted stellar signal was about 10% of the total H Ly α signal or about 120 R. Because neither the absolute stellar H Ly α emission intensity nor the LISM H Ly α extinction are known a priori, we believe that relating the H Ly α flux to the stellar continuum flux between 950 and 1170 Å only yields stellar background H Ly α intensities accurate to about 35%. Therefore the absolute error for the most contaminated integration elements is about 40 R. Also apparent in Figure A1 is a bright patch associated with the planet itself. These are the H_2 Lyman and Werner band emissions from the bright crescent of the planet (Figure 2).

H Ly α Background

Solar H Ly α photons resonantly scattered in the LISM are by far the strongest source of background signal. Both the spatial and the temporal variations of LISM H Ly α intensities are reviewed and modelled by *Ajello et al.* [1987]. The *Ajello et al.* [1987] model is used to calculate the shape of the LISM H Ly α background which we scale to best match the intensities around the perimeter of our mosaic and subtract from the data. The calculated shape is very nearly

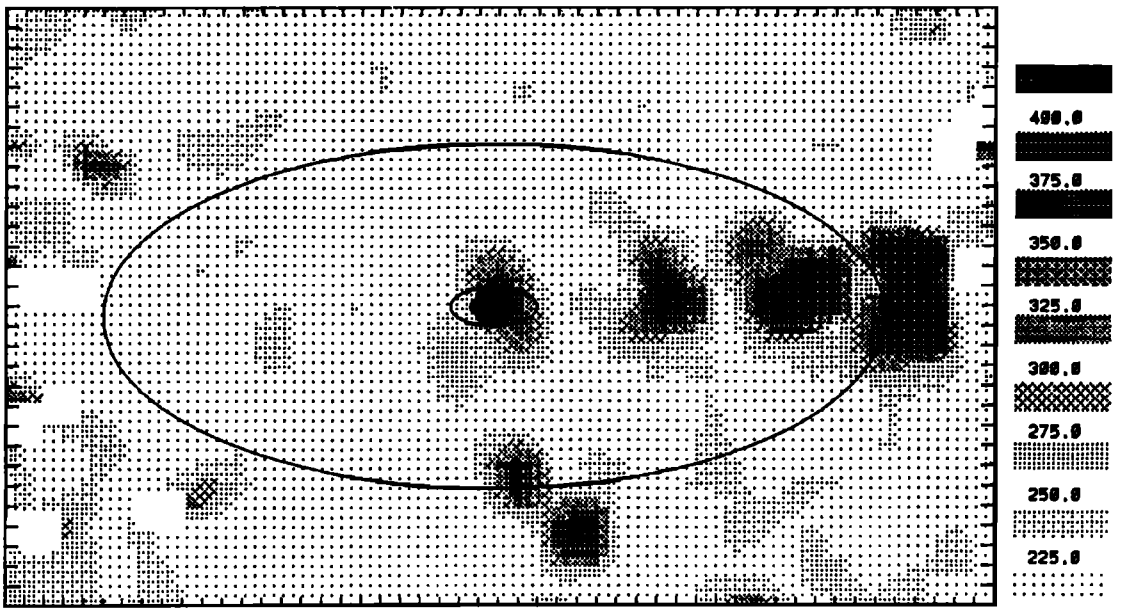

Fig. A1. Half tone plot of stellar continuum intensities (950–1150 Å) obtained from Voyager 1 UVS mosaic scans of the Saturn system conducted during the period 1980 DOY 324 and 343. Stellar background signal in the H Ly α channels is calculated using a correlation to the observed continuum signal in the wavelength range 950–1150 Å. The most contaminated pixels correspond to about 120 R H Ly α background. (The intensity scale is in relative units.)

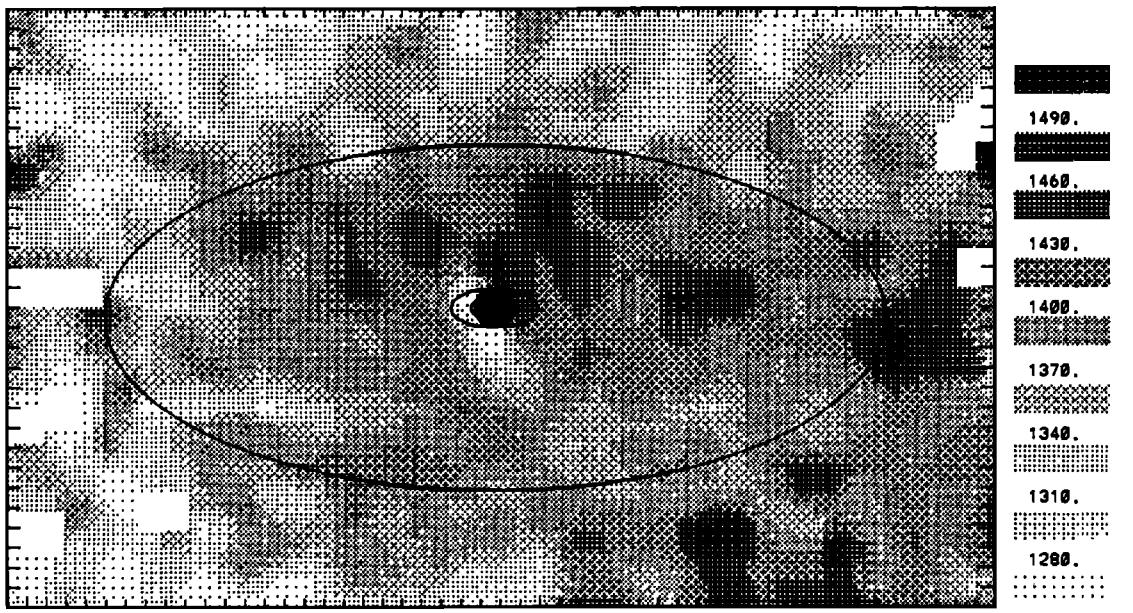

Fig. A2. Half tone plot of the total H Ly α intensities observed by Voyager 1 during scans conducted during the period 1980 DOY 324 to 343. Only UVS dark counts and stellar continuum are removed as background. The observed signal is due to solar H Ly α resonance scattering from neutral hydrogen in both the LISM and the Saturn system. The intensity scale given on right is in Rayleighs. The decreased brightness in the immediate vicinity of the planet is caused by obscuration of the LISM by Saturn and its rings.

planar over the solid angle covered in the mosaic scans. In fact, this model background shape can be replaced with a tilted planar background empirically fitted to the periphery of the data with very little change in the resultant H Ly α image. In Figure A2 the H Ly α image is shown without any LISM background subtracted (only calibration plate and stellar backgrounds are removed). The arrow shows the incoming solar flux direction. Figure 1*a* shows the corresponding image with the model H Ly α background subtracted. The mean brightness of the subtracted background is about 1275 R leaving a residual Saturnian system signal peaking just below 200 R.

The *Ajello et al.* [1987] model approximates the LISM H Ly α intensity by calculating a line of sight integral through the H distribution given by *Thomas* [1978]. The *Thomas* [1978] "hot" H distribution consists of a uniform interstel-

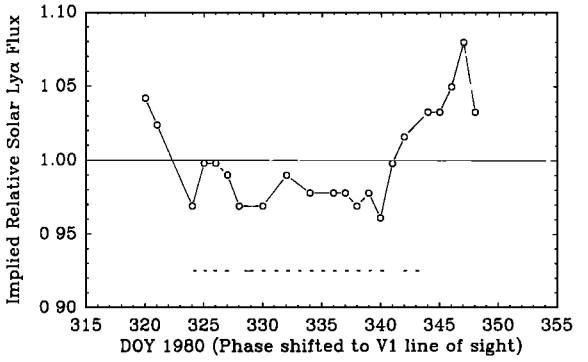

Fig. A3. Normalized solar H Ly α flux implied by He 10830 Å chromospheric equivalent width measurements (shifted appropriately in phase to Voyager 1 line of sight). The mosaic scans were

lar medium flowing through the solar system in which solar ionizing radiation and solar wind charge exchange produce a cavity in the H distribution elongated in the downstream direction. The H Ly α model approximates the effects of multiple scattering by using the Monte Carlo radiative transfer results from *Keller et al.* [1979, 1981] and includes the effects of solar wind latitudinal variation [*Witt et al.* 1979]. The free parameters that determine the cavity geometry are taken from *Ajello et al.* [1987] as follows: (1) an ambient ISM H temperature of 10^4 K, (2) a relative velocity of the ISM and the solar system of 22.5 km s^{-1} (downstream direction $\alpha = 72°$ and $\delta = 17°$), (3) the ratio of radiation pressure force to gravitational force experienced by a hydrogen atom, $\mu = 1.0$, and finally (4) the lifetime of a neutral hydrogen atom at 1 AU determined by solar wind charge exchange and photoionization, 1.29×10^6 s.

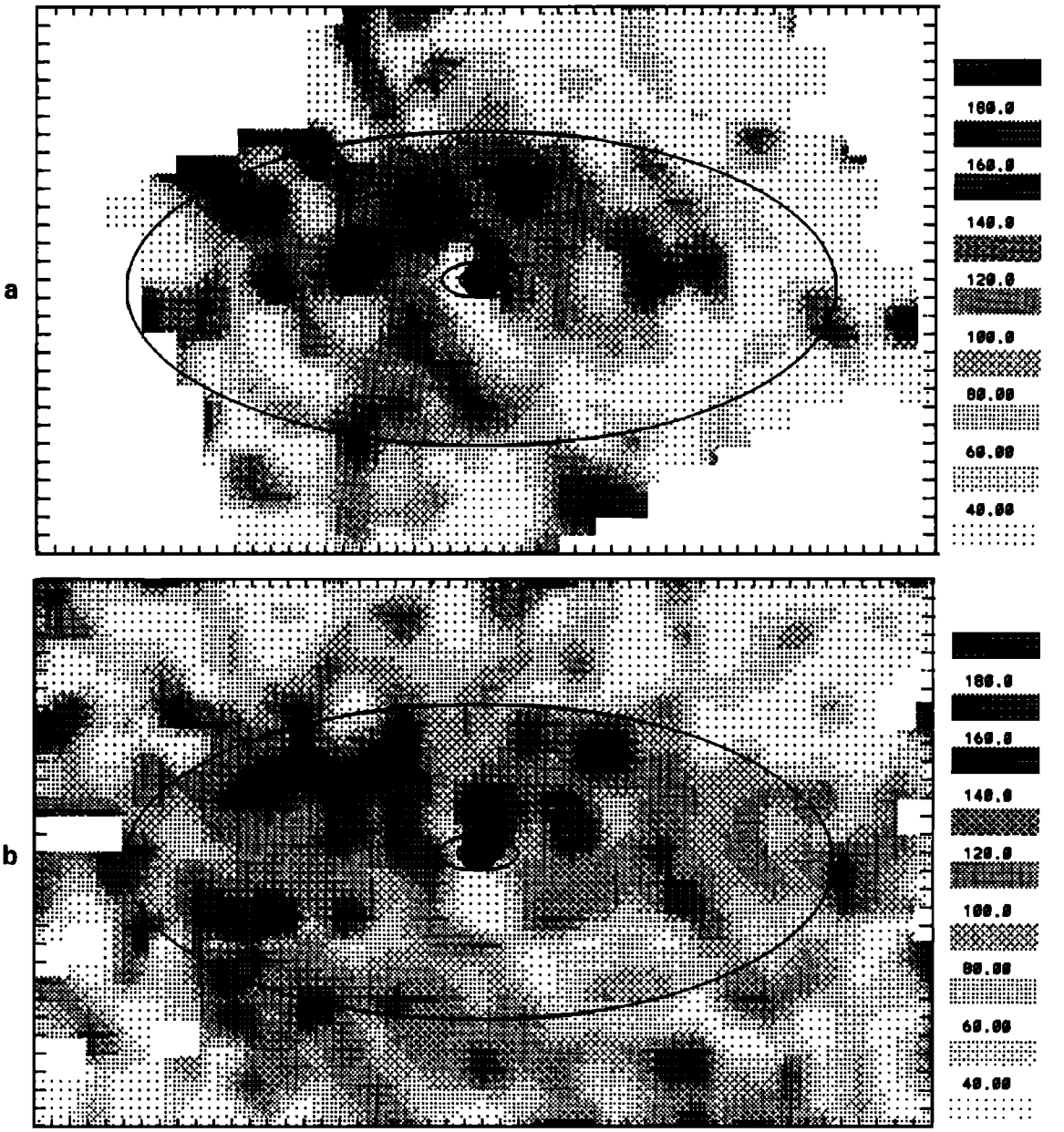

Fig. A4. (*a*) Half tone plot of the Saturn system H Ly α intensities obtained from scans conducted during the period 1980 DOY 324 to 329 (44.3 hours accumulated exposure time). (*b*) Similar plot of intensities obtained from scans conducted between DOY 330 and 343 (82 hours accumulated exposure time). These images are reduced and processed exactly as in Figure 1*a* in the main text which combines all of the scans. They are shown here to illustrate the reproducibility of the scan data. Pixels with no data are left blank.

Because of the angular contraction of the system with time the earliest scans tended to preferentially sample the inner parts of the system, and the outer region was defined mostly by the later scans. If the solar H Ly α center line flux varied significantly over this period, a systematic bias between inner and outer system intensities could be introduced. During 1980 there were no direct observations made of either solar H Ly α integrated or line center flux. However, the integrated solar H Ly α flux correlates very well with observed Helium 10830 Å equivalent width measurements [*Donnelly et al.* 1986; *Skinner et al.* 1988]. Also the H Ly α line shape appears to remain constant over the solar cycle [*Ajello et al.* 1987; *Shemansky et al.* 1984]. In Figure A3 the predicted solar H Ly α flux variations are plotted on a normalized scale. The periods when the mosaic scans were conducted are marked below the data. The solar H Ly α variation is less than 5% and shows no increasing or decreasing trend over these periods. This justifies the use of a "snapshot" LISM H Ly α background model rather than a more complicated time dependent approach. During the accumulation process we tabulated the average right ascension and declination of each integration element in the summation plane. Subsequently, these average values were to calculate the LISM background shape which was scaled to match the observed intensities at distances greater than 6 Saturn radii outside Titan's orbital ellipse.

These scans were conducted using the airglow mode of the Voyager UVS instrument [*Broadfoot et al.* 1977]. However, the UVS occultation port admits photons into the instrument even when observing in the airglow mode. The occultation port aperture is offset 19.5° in scan platform elevation relative to the airglow port. In the H Ly α channels (numbers 70 through 78) the signal observed in the airglow mode is due to the flux incident on the airglow port plus 6.6% of the flux on the occultation port. We have included the occultation port H Ly α contamination in the calculated background.

The calculated background shape is basically planar over the angular extent of the mosaic region. The background image in H Ly α emission is very insensitive to LISM parameters because of the small angular extent of the scans (<10°).

Statistical Errors

The UVS is a photon-counting instrument and any measured signal is subject to statistical errors. A plot of the statistical errors is presented in Figure 1*b*. Inside Titan's orbital ellipse the errors are generally 40 R or less whereas the observed residual Saturn system emissions are generally 120 R or greater giving a signal-to-noise ratio about 3 or 4. This explains the somewhat noisy appearance of the Ly α image as well as the need to perform a 1-2-1; 2-4-2; 1-2-1 two-dimensional smoothing on the residual intensities. The signal-to-noise ratio is much poorer at the periphery of the image because the scan sequencing concentrated on the interior region. However, the entire peripheral area is used in the normalization of the background image, giving a statistical uncertainty in background level of about ±15 R.

In Figure A4*a* the residual H Ly α emissions are plotted for the scans performed between 1980 DOY 324 and 329 (44.3 hours total scan time). Similarly, Figure A4*b* corresponds to the period 1980 DOY 330–343 (82.0 hours). These subcomponent images have been reduced and plotted exactly as the combined image, Figure 1*a*. By splitting the accumulated scans into two parts, two points are illustrated. First, from Figure A4*a* one can see that the earlier scans did indeed preferentially sample the interior of the system. And second, the overall qualitative similarity between the final combined image and the two subcomponents raises the credibility of the final result. Note that there are specific localized differences between the two images. However, the bulk emission located inside Titan's orbital ellipse and between hour angles 1200 and 2400 in the Saturn system is strong in both images. We conclude that the observed distribution is real, within statistical uncertainty.

APPENDIX B: VOYAGER UVS SATURN PREENCOUNTER SCANS

This appendix briefly describes the data compiled to produce Figures 8 and 10 of the main text. The representative scan geometries for these scans are shown in Figures 7 and 9, respectively.

Voyager 1 Preencounter Scans

Table B1 lists the dates, scan durations, and FDSC ranges for Voyager 1 scans compiled to create Figure 8 of the main text. The data were gathered during the period 1980 DOY 239 to 256 during which time the spacecraft-planet range varied from 1740 to 1370 R_S. A representative scan conducted on DOY 244 is illustrated in Figure 7. A constant LISM background of ≈ 1100 R was subtracted from the data in Figure 8. In addition, the planetary Ly α signal has been removed by subtracting a scaled version of planetary H_2 band emissions in the wavelength region 950 to 1100 Å . The uncertainty of this removal is reflected in the large error bars in Figure 8 within 3 R_S of the planet.

TABLE B1. Voyager 1 Saturn Preencounter Scan Information

Onset 1980, DOY	Δt hours	Initial FDS Count	Final FDS Count
239	13.51	32577:30	32594:23
240	16.00	32605:00	32625:00
241	13.47	32636:34	32653:24
242	13.48	32667:21	32684:12
243	13.49	32695:34	32712:26
244	13.51	32726:22	32743:15
245	17.60	32755:00	32777:00
246	17.60	32785:00	32807:00
247	11.41	32815:00	32829:16
248	13.49	32844:26	32861:18
249	13.11	32875:14	32891:37
250	16.00	32905:00	32925:00
251	13.51	32934:16	32951:09
252	16.00	32965:00	32985:00
253	...	...	...
254	13.51	33024:06	33040:59
255	16.00	33055:00	33075:00
256	9.39	33085:42	33097:26

Voyager 2 Preencounter Scans

Table B2 lists the pertinent data for Voyager 2 scans compiled to create Figure 10 of the main text. The data were gathered over the period 1981 DOY 180 to 186 and spacecraft-planet ranges 920 to 820 R_S. A representative scan conducted on DOY 185 is shown in Figure 9 of the main text. A constant LISM background of ≈800 R was subtracted from the data in Figure 10. The planetary Ly α signal has been removed in the same fashion as for the Voyager 1 scans.

TABLE B2. Voyager 2 Saturn Preencounter Scan Information

Onset 1981, DOY	Δt hours	Initial FDS Count	Final FDS Count
180	4.6	42260:03	42265:46
181	14.0	42289:10	42306:41
182	14.0	42318:35	42336:06
183	14.0	42350:07	42367:37
184	14.0	42379:16	42396:46
185	14.0	42408:25	42425:55
186	14.0	42437:35	42455:06

Acknowledgments. The authors acknowledge useful discussion with J. D. Richardson, A. Eviatar, D. M. Hunten, D. Hilton, and D. F. Strobel. The authors thank P. L. Matheson for inserting water chemistry reactions into our plasma code. This research is supported by NASA, Division of Planetary Sciences, grant NAGW-649, to the University of Arizona.

The Editor thanks A. Eviatar and another referee for their assistance in evaluating this paper.

REFERENCES

Ajello, J. M., A. I. Stewart, G. E. Thomas, and A. Graps, Solar cycle study of interplanetary Lyman–alpha variations: Pioneer Venus orbiter sky background results, *Astrophys. J.*, *317*, 964–986, 1987.

Barbosa, D. D., Radial Diffusion of low-energy plasma ions in Saturn's magnetosphere, *J. Geophys. Res.*, *95*, 17,167–17,177, 1990.

Barker, E., S. Cazes, C. Emerich, A. Vidal-Madjar, and T. Owen, Lyman alpha observations in the vicinity of Saturn with Copernicus, *Astrophys. J.*, *242*, 383–394, 1980.

Bridge, H. S., et al., Plasma observations near Saturn: Initial results from Voyager 1, *Science*, *212*, 217–224, 1981.

Bridge, H. S., et al., Plasma observations near Saturn: Initial results from Voyager 2, *Science*, *215*, 563–570, 1982.

Broadfoot, A. L., et al., Ultraviolet spectrometer experiment for the Voyager mission, *Space Sci. Rev.*, *21*, 183–205, 1977.

Broadfoot, A. L., et al., Extreme ultraviolet observations from Voyager 1 encounter with Saturn, *Science*, *212*, 206–211, 1981.

Carlson, R. W., Photo-sputtering of ice and hydrogen around Saturn's rings, *Nature*, *283*, 461, 1980.

Clarke, J. T., H. W. Moos, S. K. Atreya, and A. L. Lane, IUE detection of bursts of H Ly α emission from Saturn, *Nature*, *290*, 226–227, 1981.

Donnelly, R. F., H. E. Hinteregger, and D. F. Heath, Temporal variations of solar EUV, UV, and 10830 Å radiations, *J. Geophys. Res.*, *91*, 5567–5578, 1986.

Eviatar, A., Plasma in Saturn's magnetosphere, *J. Geophys. Res.*, *89*, 3821–3828, 1984.

Eviatar, A., and J. D. Richardson, Water group plasma in the magnetosphere of Saturn, *Ann. Geophys.*, *8*, 725–732, 1990.

Frank, L. A., B. G. Burek, K. L. Ackerson, J. H. Wolfe, and J. D. Mihalov, Plasmas in Saturn's magnetosphere, *J. Geophys. Res.*, *85*, 5695–5708, 1980.

Hilton, D. A., and D. M. Hunten, A partially collisional model of the Titan hydrogen torus, *Icarus*, *73*, 248–268, 1988.

Holberg, J. B., Far-ultraviolet background observations at high galactic latitude, II, Diffuse emission, *Astrophys. J.* , *311*, 969–978, 1986.

Hood, L. L., Radial diffusion and losses of energetic protons in the 5 to 12 R_S region of the Saturn magnetosphere, *J. Geophys. Res.*, *94*, 8721–8730, 1989.

Hunten, D. M., Titan's atmosphere and surface, in *Planetary Satellites*, edited by J. A. Burns, pp. 420–437, University of Arizona Press, Tucson, 1977.

Ip, W.-H., An estimate of the H2 density in the atomic hydrogen cloud of Titan, *J. Geophys. Res.*, *89*, 2377–2379, 1984.

Ip, W.-H., Nitrogen tori of Titan and Triton, paper presented at the 5'th Symposium on Magnetospheres of the Outer Planets: Comparative Studies, Comm. on Space Res., The Hague, 1990.

Johnson, R. E., Application of laboratory data to the sputtering of a planetary regolith, *Icarus*, *78*, 206–210, 1989.

Johnson, R. E., M. K. Pospieszalska, E. C. Sittler, A. F. Cheng, L. J. Lanzerotti, and E. M. Sieveka, The neutral cloud and heavy ion inner torus at Saturn, *Icarus*, *77*, 311–329, 1989.

Judge, D. L., F. M. Wu, and R. W. Carlson, Ultraviolet photometer observations of the Saturnian system, *Science*, *207*, 431–434, 1979.

Keller, H. U., and G. E. Thomas, Multiple scattering of solar resonance radiation in the nearby interstellar medium, I, *Astron. Astrophys.*, *80*, 227–233, 1979.

Keller, H. U., K. Richter, and G. E. Thomas, Multiple scattering of solar resonance radiation in the nearby interstellar medium, II, *Astron. Astrophys.*, *102*, 415–423, 1981.

McDonough, T. R., and N. M. Brice, A Saturnian gas ring and the recycling of Titan's atmosphere, *Icarus*, *20*, 136–145, 1973.

Pospieszalska, M. K., and R. E. Johnson, Magnetospheric ion bombardment profiles of satellites: Europa and Dione, *Icarus*, *78*, 1–13, 1989.

Richardson, J. D., and A. Eviatar, Limits on the extent of Saturn's hydrogen cloud, *Geophys. Res. Lett.*, *14*, 999–1002, 1987.

Richardson, J. D., and A. Eviatar, Observational and theoretical evidence for anisotropies in Saturn's magnetosphere, *J. Geophys. Res.*, *93*, 7297–7306, 1988.

Richardson, J. D., and E. C. Sittler, A plasma density model for Saturn based On Voyager observations, *J. Geophys. Res.*, *95*, 12,019–12,031, 1990.

Richardson, J. D., A. Eviatar, and G. L. Siscoe, Satellite tori at Saturn, *J. Geophys. Res.*, *91*, 8749–8755, 1986.

Sandel, B. R., et al., Extreme ultraviolet observations from Voyager 2 encounter with Saturn, *Science*, *215*, 548–553, 1982.

Shemansky, D. E., An explanation for the H Ly α longitudinal asymmetry in the equatorial spectrum of Jupiter: An outcrop of paradoxical energy deposition in the exosphere, *J. Geophys. Res.*, *90*, 2673–2694, 1985.

Shemansky, D. E., Energy branching in the Io plasma torus, *J. Geophys. Res.*, *93*, 1773–1784, 1988.

Shemansky, D. E., and D. T. Hall, Atomic hydrogen in the magnetosphere of Saturn and Uranus, *Bull. Am. Astron. Soc.*, *19*, 850, 1987.

Shemansky, D. E., and G. R. Smith, Whence comes the "Titan" hydrogen torus?, *EOS Trans. AGU*, *63*, 1019, 1982.

Shemansky, D. E., and G. R. Smith, The implication for the presence of a magnetosphere on Uranus in the relationship of EUV and radio emission, *Geophys. Res. Lett.*, *13*, 2–5, 1986.

Shemansky, D. E., D. L. Judge, and J. M. Jessen, Pioneer 10 and Voyager observations of the interstellar medium in scattered emission of the He 584 Å and H Ly α 1216 Å lines, in *Local Interstellar Medium NASA CP 2345*, edited by Y. Kondo, F. C. Bruhweiler, and B. D. Savage, pp. 24–27 , International Astronomical Union, Madison, Wis., 1984.

Shemansky, D. E., G. R. Smith, and D. T. Hall, Extended atomic hydrogen cloud in the Saturn system, and a possible analogous distribution at Uranus, *EOS Trans. AGU*, *66*, 1008, 1985.

Skinner, T. E., M. T. DeLand, G. E. Ballester, K. A. Coplin, P. D. Feldman, and H. W. Moos, Temporal Variation of the Jovian HI Lyman alpha emission 1979–1986, *J. Geophys. Res.*, *93*, 29–34, 1988.

Smith, G. R., D. F. Strobel, A. L. Broadfoot, B. R. Sandel, D. E. Shemansky, and J. B. Holberg, Titan's Upper Atmosphere: Composition and temperature from the EUV solar occultation results, *J. Geophys. Res.*, *87*, 1351–1359, 1982.

Smyth, W. H., Titan's hydrogen torus, *Astrophys. J.*, *246*, 344–353, 1981.

Spitzer, L., *Physics of Fully Ionized Gases*, pp. 120–154, John Wiley, New York, 1962.

Thomas, G. E., The interstellar wind and its influence on the interplanetary environment, *Earth Planet. Sci.*, *6*, 173–204, 1978.

Weiser, H., R. C. Vitz, and H. W. Moos, Detection of Lyman alpha emission from the Saturnian disk and from the ring system, *Science*, *197*, 755–757, 1977.

Witt, N., J. M. Ajello, and P. W. Blum, Solar wind latitudinal variations deduced from Mariner 10 interplanetary H (1216 Å) observations, *Astron. Astrophys.*, *73*, 272–281, 1979.

Wu, F. M., K. Suzuki, R. W. Carlson, and D. L. Judge, Pioneer 10 ultraviolet photometer observations of the interplanetary glow at heliocentric distances from 2 to 14 AU, *Astrophys. J.*, *245*, 1145–1158, 1981.

D. T. Hall, Lunar and Planetary Laboratory-West, University of Arizona, Gould-Simpson Building, Rm 927, Tucson, AZ 85721.

D. E. Shemansky, Department of Aerospace Engineering, USC, 854 W. 36th Place, Los Angeles, CA 90089-1191.

(Received March 22, 1989;
revised October 24, 1991;
accepted October 29, 1991.)